NJC

PAPER

View Article Online
View Journal | View Issue

Cite this: *New J. Chem.*, 2019, 43, 16714

Synthesis, characterization, and cytotoxic and antimicrobial activities of mixed-ligand hydrazone complexes of variable valence VO^{z+} (*z* = 2, 3)†

Nirmalendu Biswas,[a] Sachinath Bera,[b] Nayim Sepay,[b] Titas Kumar Mukhopadhyay,[c] Krishnendu Acharya,[d] Sandipta Ghosh,[d] Swarnali Acharyya,[e] Anup Kumar Biswas,[f] Michael G. B. Drew[g] and Tapas Ghosh *[a]

Two sets of mixed-ligand complexes were synthesized and characterized, namely, $[V^{IV}O(L^{1-4})(phen)]$ (**1–4**) and $[V^{V}O(L^{1-4})(hq)]$ (**5–8**) incorporating 2-aminobenzoylhydrazone of 2-hydroxyacetophenone (H_2L^1), 2-hydroxy-5-methylacetophenone (H_2L^2), 2-hydroxy-5-methoxyacetophenone (H_2L^3) and 5-chloro-2-hydroxyacetophenone (H_2L^4) as primary ligands together with 1,10-phenanthroline (phen) and 8-hydroxyquinoline (Hhq) as co-ligands. The complexes were characterized by elemental analyses, magnetic susceptibility measurements and various spectroscopic techniques. The structures of complexes **2**, **5** and **8** were determined by single crystal X-ray diffractometry. This study indicates that the co-ligands have remarkable effects on the selective stabilization of the oxidation state of vanadium because the neutral N,N donor phen ligand stabilizes the +IV state, while the monobasic O^-,N donor hq^- ligand stabilizes the +V state. Substituents on the aryloxy ring also had significant effects on the electronic properties of vanadium in the resulting complexes. The $E_{1/2}$ values of all the complexes and the λ_{max} values for the LMCT transitions of pentavalent complexes **5–8** exhibited linear relationships with the Hammett parameter of the substituent. The complexes exhibited promising cytotoxic activity against lung cancer cells. Interestingly, complexes **2**, **3** and **4** (with IC_{50} values of *ca.* 2.5 μM) exhibited cytotoxic activity comparable to that found for the widely used cisplatin (also with an IC_{50} value of 2.5 μM). Nuclear staining experiments suggest that the complexes kill the cells through apoptosis, which is further substantiated by molecular docking studies. These complexes also exhibited potential antimicrobial activity against *Escherichia coli*, *Bacillus subtilis*, *Staphylococcus aureus* and *Salmonella typhimurium*.

Received 11th August 2019,
Accepted 1st October 2019

DOI: 10.1039/c9nj04171k

rsc.li/njc

1. Introduction

Vanadium is an important trace bio-element with a variety of oxidation states, ranging from −III to +V and has rich coordination chemistry.[1] In its two higher (+IV and +V) oxidation states, vanadium is oxophilic and forms a variety of oxido species, *viz.*, VO^{2+}, VO^{3+}, $(OV\text{-}\mu\text{-}O\text{-}VO)^{3+/4+}$ [*i.e.*, $(V_2O_3)^{3+/4+}$] and VO_2^+ involving extremely strong and inert V≡O bonds.[2,3]

[a] *Post Graduate Department of Chemistry, Ramakrishna Mission Vivekananda Centenary College, Rahara, Kolkata-700118, India. E-mail: ictg_64@yahoo.co.in*
[b] *Department of Chemistry, Jadavpur University, Kolkata 700032, India*
[c] *Department of Spectroscopy, Indian Association for the Cultivation of Science, Jadavpur, Kolkata-700032, India*
[d] *Department of Botany, University of Calcutta, 35, Ballygunge Circular Road, Kolkata-700019, India*
[e] *Department of Pathology and Cell Biology, Columbia University, New York, NY, USA*
[f] *Herbert Irving Comprehensive Cancer Centre, Columbia University, 1130 St. Nicholas Avenue, New York, NY 10032, USA*
[g] *Department of Chemistry, The University of Reading, PO Box 224, Whiteknights, Reading, RG6 6AD, UK*

† Electronic supplementary information (ESI) available: Molecular structure of **2** with ellipsoids at 30% probability. The intramolecular hydrogen bond is shown as a dotted line (Fig. S1), overlay of the electronic spectra of complexes **1–4** in CH_2Cl_2 solution (Fig. S2), overlay of the electronic spectra of complexes **5–8** in CH_2Cl_2 solution (Fig. S3), ^{51}V NMR of complexes **5–8** in $CDCl_3$ solution at 298 K (Fig. S4), X-band EPR spectra of complexes **1**, **3** and **4** (black, experimental; red, simulated) in CH_2Cl_2 solution at (a) 300 K and (b) 77 K (Fig. S5–S7 respectively), schematic diagram of selected frontier orbitals for complexes **1–8** in their ground state geometries (Fig. S8), cytotoxic activity of the H_2L^{1-4} ligands (Fig. S9), cytotoxic activity of $[V^{IV}O(aa)_2]$ (Fig. S10), cytotoxic activity of 1,10-phenanthroline and 8-hydroxyquinoline (Fig. S11), two dimensional representations of binding sites interacting with the molecules of (a) **3** and (b) **6** (Fig. S12), dose–response curves for the antimicrobial activity of complex **2** (Fig. S13), dose–response curves for the antimicrobial activity of complex **5** (Fig. S14), calculated geometrical parameters for complexes **1–4** (Table S1), calculated geometrical parameters for complexes **5–8** (Table S2). LD_{50} on a lung cancer cell line and binding energies of compounds **1–8** with Bcl2 protein (Table S3). CCDC 1887600–1887602. For ESI and crystallographic data in CIF or other electronic format see DOI: 10.1039/c9nj04171k

Of them, the oxidovanadium ion represents the most stable diatomic cation and dominates the chemistry of vanadium. The selective stabilization of these two states (namely, +IV and +V) in a complex depends on the basicity of the donor moieties of the ligand and the pH of the reaction medium. Vanadium has several effects on organisms; the following properties are remarkable: (i) a stimulatory effect on the growth of algae and plants,[4] (ii) the inhibitory action of vanadate(v) on Na,K-ATPase,[5] (iii) the involvement of vanadate in the regulation of phosphate metabolism in human organisms,[6] (iv) the presence of vanadium at the active site of certain enzymes, including haloperoxidases in sea algae and lichens and some nitrogenases in the nitrogen-fixing Azotobacter.[7] It has been observed that vanadium complexes have a wide range of therapeutic potentials, *e.g.*, insulin enhancing,[8] antiamoebic[9] and antitumor[10] activities. During the last ten years or so, our group has been working on the chemistry of vanadium[11] utilizing different types of hydrazone ligands which, being derived from the condensation of aliphatic/aromatic acid hydrazides with aliphatic/aromatic carbonyl compounds, are versatile multidentate O,N donor ligands and have a wide range of applications in the fields of analytical[12] and medicinal[13] chemistry. Hydrazone moieties provide important pharmaceutical cores for several anti-cancer, anti-inflammatory and anti-platelet drugs.[14] Moreover, such types of hydrazone ligands contain O/N donor atoms which are essential in stabilizing the +IV and +V states of vanadium due to their hard acidic nature.

The electronic properties of a metal ion in a complex can be tuned by changing the co-ordination environment around the metal ion and this can be done by two ways in a mixed-ligand system: (i) by making substitutions on either or both of the coordinated ligands or (ii) by changing one ligand, so varying basicity. From this perspective, we have used a family of hydrazone ligands which are derived by the condensation of 2-aminobenzoylhydrazide with 2-hydroxyacetophenone and its 5-substituted derivatives (H_2L^{1-4}, general abbreviation H_2L, Scheme 1) with a view to studying the effect of substituents on the electronic properties of the metal. In addition, to study the effect of auxiliary ligands on the oxidation state of vanadium in the presence of the above mentioned hydrazone ligands 1,10-phenanthroline (phen, a neutral NN donor) and 8-hydroxyquinoline (Hhq, a monobasic ON donor) have been used. It has been found that starting from a tetravalent precursor $[V^{IV}O(aa)_2]$ [where aa^- represents the monoanionic form of acetylacetone (Haa)] in the presence of phen, the H_2L^{1-4} ligands yielded the tetravalent complexes $[V^{IV}O(L^{1-4})(phen)]$ (**1–4**), while the pentavalent complexes $[V^{V}O(L^{1-4})(hq)]$ (**5–8**) were obtained in the presence of Hhq. These types of tetravalent and pentavalent mixed-ligand complexes are very rare particularly in the presence of hydrazone ligands.[11,15–17] These complexes were characterized by elemental analyses and by various spectroscopic techniques, namely, IR, UV-vis, ^{1}H NMR, ^{51}V NMR and ESR, and also by magnetic susceptibility measurements. Complexes **2**, **5** and **8** were structurally characterized by X-ray crystallography. To the best of our knowledge, complex **2** represents the first structurally characterized complex containing hydrazone as the primary ligand and phen as the auxiliary ligand. The electrochemical behaviour of these complexes was studied by cyclic voltammetry. The complexes were screened for cytotoxic activity against lung cancer cells and antimicrobial activity against four pathogenic bacterial strains.

2. Experimental and computational

2.1 Materials and methods

2-Hydroxyacetophenone, 2-hydroxy-5-methylacetophenone, 2-hydroxy-5-methoxyacetophenone and 5-chloro-2-hydroxyacetophenone were obtained from Aldrich. 2-Aminobenzoylhydrazide was purchased from E. Merck. Acetylacetone and vanadyl sulphate pentahydrate were obtained from Loba Chemical Company (India). $[V^{IV}O(aa)_2]$ was prepared by a previously reported method.[18] All other reagents were of A. R. grade obtained from commercial sources and used without further purification.

2.2 Synthesis of H_2L^{1-4} ligands

These ligands were synthesised in good yield by refluxing 2-aminobenzoylhydrazide with the respective 2-hydroxyacetophenone in an equimolar ratio in methanol as described

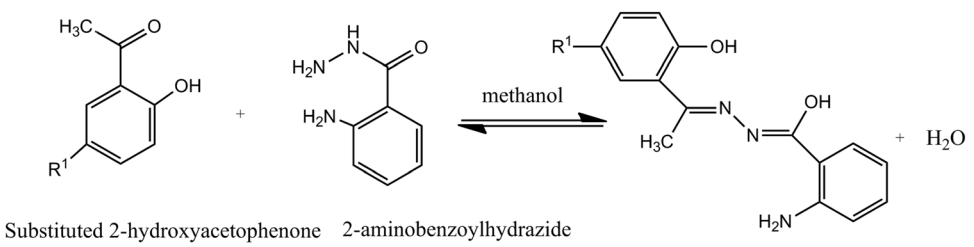

$R^1 = H, H_2L^1$

$R^1 = CH_3, H_2L^2$

$R^1 = OCH_3, H_2L^3$

$R^1 = Cl, H_2L^4$

Scheme 1 Hydrazone ligands used in this study.

elsewhere.[19] Elemental analyses, ^{1}H NMR, IR and mass spectral data confirmed their identity.

2.3 Synthesis of $[V^{IV}O(L^{1-4})(phen)]$ (1–4) complexes

2.3.1 $[V^{IV}O(L^1)(phen)]$ (1). To a methanolic solution (20 mL) of $[V^{IV}O(aa)_2]$ (0.265 g, 1.00 mmol) was added a warm methanolic solution (20 mL) of H_2L^1 (0.27 g, 1.00 mmol) dropwise with stirring. The reaction mixture was then heated under reflux for 2 h. After cooling the reaction mixture to room temperature, a methanolic solution (10 mL) of phen (0.180 g, 1.00 mmol) was added dropwise with continuous stirring. Immediately the brown solution turned orange. The reaction mixture was then stirred at room temperature for 1 h. A shiny orange-red microcrystalline product was obtained after stirring the reaction mixture for 1 h at room temperature, and was filtered, washed with methanol and dried over silica gel. Yield: 0.41 g (79% based on $[V^{IV}O(aa)_2]$). Anal. calcd for $C_{27}H_{21}N_5O_3V$: C, 63.03%; H, 4.08%; N, 13.62%. Found: C, 62.91%; H, 4.21%; N, 13.55%. FT-IR bands (KBr pellet, cm^{-1}): 3360 (N–H), 1614, 1597 (C═$N_{azomethine}$), 1371 (C–$O_{phenolic}$), 1244 (C–O_{enolic}), 1013 (N–N), 958 (V≡O). UV-Vis (CH_2Cl_2) [λ_{max}, nm (ε, M^{-1} cm^{-1})]: 851 (40), 755 (40), 410 (12 380), 321 (12 230). ESI-MS (positive) in CH_3CN: 515.39 ($M + H^+$; actual mass = 515.44), 537.39 ($M + Na^+$; 537.44).

2.3.2 $[V^{IV}O(L^2)(phen)]$ (2). This compound was prepared following an identical procedure to that described for compound **1** using the ligand H_2L^2 instead of H_2L^1. Yield: 0.40 g (76%). Anal. calcd for $C_{28}H_{23}N_5O_3V$: C, 63.64%; H, 4.36%; N, 13.25%. Found: C, 63.45%; H, 4.46%; N, 13.14%. FT-IR bands (KBr pellet, cm^{-1}): 3358 (N–H), 1615, 1586 (C═$N_{azomethine}$), 1371 (C–$O_{phenolic}$), 1262 (C–O_{enolic}), 1043 (N–N), 959 (V≡O). UV-Vis (CH_2Cl_2) [λ_{max}, nm (ε, M^{-1} cm^{-1})]: 842 (30), 774 (30), 409 (13 630), 322 (15 720). ESI-MS (positive) in CH_3CN: 528.96 ($M + H^+$; 529.45), 550.94 ($M + Na^+$; 551.45).

2.3.3 $[V^{IV}O(L^3)(phen)]$ (3). This compound was prepared following an identical method to that described for compound **1** using the ligand H_2L^3 instead of H_2L^1. Yield: 0.39 g (73%). Anal. calcd for $C_{28}H_{23}N_5O_4V$: C, 61.76%; H, 4.23%; N, 12.87%. Found: C, 61.62%; H, 4.30%; N, 12.79%. FT-IR bands (KBr pellet, cm^{-1}): 3399 (N–H), 1616, 1585 (C═$N_{azomethine}$), 1365 (C–$O_{phenolic}$), 1260 (C–O_{enolic}), 1027 (N–N), 956 (V≡O). UV-Vis (CH_2Cl_2) [λ_{max}, nm (ε, M^{-1} cm^{-1})]: 840 (30), 724 (30), 406 (8530), 322 (16 670). ESI-MS (positive) in CH_3CN: 545.06 ($M + H^+$; 545.46).

2.3.4 $[V^{IV}O(L^4)(phen)]$ (4). This compound was prepared following an identical method to that described for compound **1** using the ligand H_2L^4 instead of H_2L^1. Yield: 0.44 g (79%). Anal. calcd for $C_{27}H_{20}N_5O_3ClV$: C, 59.13%; H, 3.65%; N, 12.77%. Found: C, 58.91%; H, 3.76%; N, 12.66%. FT-IR bands (KBr pellet, cm^{-1}): 3374 (N–H), 1614, 1592 (C═$N_{azomethine}$), 1372 (C–$O_{phenolic}$), 1259 (C–O_{enolic}), 1038 (N–N), 958 (V≡O). UV-Vis (CH_2Cl_2) [λ_{max}, nm (ε, M^{-1} cm^{-1})]: 864 (40), 720 (30), 418 (17 510), 324 (16 920). ESI-MS (positive) in CH_3CN: 549.08 (M^+; 548.88), 571.07 ($M + Na^+$; 571.88), 587.04 ($M + K^+$; 587.88).

2.4 Synthesis of $[V^{V}O(L^{1-4})(hq)]$ (5–8) complexes

2.4.1 $[V^{V}O(L^1)(hq)]$ (5). To a methanolic solution (20 mL) of $[V^{IV}O(aa)_2]$ (0.265 g, 1.00 mmol) was added a warm methanolic solution (20 mL) of H_2L^1 (0.27 g, 1.00 mmol) dropwise with stirring. The reaction mixture was then heated under reflux for 2 h. After cooling the reaction mixture to room temperature, a methanolic solution (10 mL) of Hhq (0.145 g, 1.00 mmol) was added dropwise with continuous stirring. Immediately the brown solution turned violet. The shiny black microcrystalline product obtained after stirring the reaction mixture for 1 h at room temperature was filtered, washed with methanol and dried over silica gel. Yield: 0.44 g (92% based on $[V^{IV}O(aa)_2]$). Anal. calcd for $C_{24}H_{19}N_4O_4V$: C, 60.25%; H, 3.97%; N, 11.71%. Found: C, 60.11%; H, 3.88%; N, 11.65%. FT-IR bands (KBr pellet, cm^{-1}): 3422 (N–H), 1615, 1595 (C═$N_{azomethine}$), 1368 (C–$O_{phenolic}$), 1252 (C–O_{enolic}), 1035 (N–N), 954 (V≡O). UV-Vis (CH_2Cl_2) [λ_{max}, nm (ε, M^{-1} cm^{-1})]: 545 (4320), 329 (9490). ^{1}H NMR (400 MHz, $CDCl_3$, 298 K, δ/ppm, J/Hz): 6.59 (d, 1H, H-3, J = 8.0), 7.65 (t, 1H, H-4, J = 8.0), 7.24–7.26 (m, 3H, H-5, H-11, H-20), 7.83 (d, 1H, H-6, J = 8.0), 7.09 (t, 1H, H-12, J = 8.0), 6.47 (t, 1H, H-13, J = 8.0), 7.45–7.50 (m, 2H, H-14, H-17), 2.97 (s, 3H, 3 × H-15), 7.95 (d, 1H, H-16, J = 4.0), 8.13 (d, 1H, H-18, J = 8.0), 7.02 (t, 1H, H-21, J = 8.0), 6.93 (d, 1H, H-22, J = 8.0). ^{51}V NMR (400 MHz, 293 K, δ/ppm): −480.32. ESI-MS (positive) in CH_3CN: 479.09 ($M + H^+$; 479.37), 501.08 ($M + Na^+$; 501.37), 517.05 ($M + K^+$; 517.37).

2.4.2 $[V^{V}O(L^2)(hq)]$ (6). This compound was prepared following an identical method to that described for compound **5** using the ligand H_2L^2 instead of H_2L^1. Yield: 0.42 g (85%). Anal. calcd for $C_{25}H_{21}N_4O_4V$: C, 60.97%; H, 4.27%; N, 11.38%. Found: C, 60.82%; H, 4.32%; N, 11.34%. FT-IR bands (KBr pellet, cm^{-1}): 3480 (N–H), 1616, 1575 (C═$N_{azomethine}$), 1363 (C–$O_{phenolic}$), 1256 (C–O_{enolic}), 1031 (N–N), 968 (V≡O). UV-Vis (CH_2Cl_2) [λ_{max}, nm (ε, M^{-1} cm^{-1})]: 540 (8940), 330 (20 820). ^{1}H NMR (400 MHz, $CDCl_3$, 298 K, δ/ppm, J/Hz): 6.59 (d, 1H, H-3, J = 8.0), 7.49 (dd, 1H, H-4, J = 8.0, 1.2), 7.61 (d, 1H, H-6, J = 1.2), 7.29 (dd, 1H, H-11, J = 8.0, 4.0), 7.21–7.25 (m, 2H, H-12, H-17), 6.46 (t, 1H, H-13, J = 8.0), 7.65 (d, 1H, H-14, J = 8.0), 2.94 (s, 3 × H-15), 7.93 (d, 1H, H-16, J = 4.0), 8.12 (dd, 1H, H-18, J = 8.0, 1.2), 7.44–7.46 (m, 1H, H-20), 7.08 (t, 1H, H-21, J = 8.0, 1.0), 6.83 (d, 1H, H-22, J = 8.0), 2.42 (s, 3H, 3 × H-25). ^{51}V NMR (400 MHz, 293 K, δ/ppm): −475.76. ESI-MS (positive) in CH_3CN: 493.11 ($M + H^+$; 493.41), 515.09 ($M + Na^+$; 515.41), 531.13 ($M + K^+$; 531.41).

2.4.3 $[V^{V}O(L^3)(hq)]$ (7). This compound was prepared following an identical method to that described for compound **5** using the ligand H_2L^3 instead of H_2L^1. Yield: 0.41 g (82%). Anal. calcd for $C_{25}H_{21}N_4O_5V$: C, 59.05%; H, 4.13%; N, 11.02%. Found: C, 58.92%; H, 4.26%; N, 10.92%. FT-IR bands (KBr pellet, cm^{-1}): 3566 (N–H), 1616, 1565 (C═$N_{azomethine}$), 1374 (C–$O_{phenolic}$), 1258 (C–O_{enolic}), 1044 (N–N), 955 (V≡O). UV-Vis (CH_2Cl_2) [λ_{max}, nm (ε, M^{-1} cm^{-1})]: 536 (11 140), 329 (30 830). ^{1}H NMR (400 MHz, $CDCl_3$, 298 K, δ/ppm, J/Hz): 6.87 (d, 1H, H-3, J = 8.0), 6.59 (dd, 1H, H-4, J = 8.0, J = 1.2), 7.29 (d, 1H, H-6, J = 1.2), 7.23–7.25 (m, 2H, H-11, H-17), 7.65 (t, 1H, H-12, J = 8.0), 6.47 (dt, 1H, H-13, J = 8.0, 1.2), 7.45–7.50 (m, 2H, H-14, H-21), 2.95 (s, 3H, 3 × H-15), 7.94 (dd, 1H, H-16, J = 4.0, 1.2), 8.13 (dd, 1H, H-18, J = 8.0, 1.2), 7.06–7.11 (m, 2H, H-20, H-22), 3.86 (s, 3H, 3 × H-25). ^{51}V NMR (400 MHz, 293 K, δ/ppm): −468.91. ESI-MS (positive) in CH_3CN: 509.19 ($M + H^+$; 509.41), 531.18 ($M + Na^+$; 531.41).

2.4.4 $[V^{V}O(L^{4})(hq)]$ (8). This compound was prepared following an identical method to that described for compound **5** using the ligand H_2L^4 instead of H_2L^1. Yield: 0.46 g (89%). Anal. calcd for $C_{24}H_{18}ClN_4O_4V$: C, 56.25%; H, 3.51%; N, 10.94%. Found: C, 56.10%; H, 3.39%; N, 10.87%. FT-IR bands (KBr pellet, cm^{-1}): 3445 (N–H), 1616, 1590 ($C{=}N_{azomethine}$), 1375 ($C{-}O_{phenolic}$), 1256 ($C{-}O_{enolic}$), 1024 (N–N), 975 ($V{\equiv}O$). UV-Vis (CH_2Cl_2) [λ_{max}, nm (ε, M^{-1} cm^{-1})]: 550 (6420), 332 (16 220). ^{1}H NMR (400 MHz, $CDCl_3$, 298 K, δ/ppm, J/Hz): 6.60 (d, 1H, H-3, J = 8.0), 7.39 (dd, 1H, H-4, J = 8.0, 1.2), 7.77 (d, 1H, H-6, J = 1.2), 7.27–7.29 (m, 1H, H-11), 7.66 (t, 1H, H-12, J = 8.0), 6.47 (t, 1H, H-13, J = 8.0), 7.48–7.52 (m, 2H, H-14, H-20), 2.94 (s, 3H, 3 × H-15), 7.94 (d, 1H, H-16, J = 4.0), 7.23 (d, 1H, H-17, J = 8.0), 8.15 (d, 1H, H-18, J = 8.0), 7.10 (dt, 1H, H-21, J = 8.0, 1.2), 6.87 (d, 1H, H-22, J = 8.0). ^{51}V NMR (400 MHz, 293 K, δ/ppm): −475.11. ESI-MS (positive) in CH_3CN: 512.89 (M^+; 512.81), 535.85 ($M + Na^+$; 535.81), 551.82 ($M + K^+$; 551.81).

2.5 Physical measurements

Elemental analyses were performed on a PerkinElmer 2400 CHN analyzer. IR spectra (as KBr pellets) were recorded on a Shimadzu FT-IR spectrophotometer, IR Affinity-1. Magnetic susceptibilities were measured at 298 K using a PAR model 155 vibrating sample magnetometer fitted with a Walker Scientific L75 FBAL magnet using $Hg[Co(SCN)_4]$ as the calibrant. Diamagnetic corrections were made using Pascal's constants to obtain χ_M^{corr} and the resulting μ_{eff} value was reported. The ESI-MS spectra in positive ion mode were measured on a Micromass QTOF YA 263 mass spectrometer. The X-band EPR spectra of complexes **1–4** were recorded on a Magnettech GmbH MiniScope MS400 spectrometer (equipped with temperature controller TC H03), where the microwave frequency was measured with an FC400 frequency counter. Tetracyanoethene (tcne) (g = 2.0027) was used to calibrate the EPR spectra. The EPR spectra were simulated using Easy Spin[20] software. The ^{1}H and ^{51}V NMR spectra of the complexes in $CDCl_3$ were recorded at 293 K using a Bruker AM 300L 400 MHz superconducting FT NMR spectrophotometer. The ^{51}V NMR spectra were referenced to $VOCl_3$ (0 ppm) as an external reference. The UV-vis spectra were recorded on a Shimadzu UV-1700 spectrophotometer. Electrochemical measurements were performed at 298 K in CH_2Cl_2 solution for *ca.* 1×10^{-3} mol dm^{-3} using tetrabutylammonium hexafluorophosphate (TBAHP) as supporting electrolyte under a dry N_2 atmosphere on a BASi Epsilon-EC electroanalytical instrument. A BASi platinum working electrode, a platinum auxiliary electrode and a Ag/AgCl electrode were used for measurements. The redox potential data are referenced to a ferricenium/ferrocene, Fc^+/Fc, couple.

2.6 Crystallographic data collection and refinement

X-ray quality single crystals of three complexes, namely, **2**, **5** and **8**, were obtained by the slow evaporation of the solvent CH_3OH of the respective reaction mixture at room temperature. X-ray data were measured with MoKα radiation (λ = 0.71069 Å) at 100(2) K for **2** and **8** and at 150(2) K for **5** using an Oxford Diffraction X-Calibur CCD system. Data reduction for these three complexes **2**, **5** and **8** were carried out with the CrysAlis program.[21] Structures were solved using direct methods with the Shelxs97 program.[22] The non-hydrogen atoms were refined with anisotropic thermal parameters. The hydrogen atoms bonded to carbon were included in geometric positions, and given thermal parameters equivalent to 1.2 times those of the atom to which they were attached, while those bonded to nitrogen were located in difference Fourier maps and refined with distance constraints. Absorption corrections were carried out using the ABSPACK program[23] and structures were refined on F^2 using the Shelxl16/6 program.[24] Crystallographic data are collected in Table 1. CCDC 1887600–1887602 contain the crystallographic data for complexes **2**, **5** and **8** respectively.†

Table 1 Summary of X-ray crystallographic data for complexes **2**, **5** and **8**

	2	**5**	**8**
Empirical formula	$C_{28}H_{23}N_5O_3V$	$C_{24}H_{19}N_4O_4V$	$C_{24}H_{18}ClN_4O_4V$
Formula weight	528.45	478.37	512.81
Crystal colour	Red	Black	Black
Crystal system	Triclinic	Triclinic	Monoclinic
Temperature/K	100(2)	150(2)	100(2)
Space group	$P\bar{1}$	$P\bar{1}$	$P2_1/n$
a/Å	10.2716(10)	7.8475(6)	12.6574(4)
b/Å	10.6456(9)	10.8678(9)	7.6841(2)
c/Å	12.1344(9)	14.0113(12)	22.0915(7)
α/°	81.817(7)	68.768(8)	(90)
β/°	70.266(8)	77.151(7)	91.060(3)
γ/°	82.082(7)	72.756(7)	(90)
V/Å^3	1230.48(18)	1054.86(16)	2148.27(11)
Z	2	2	4
ρ_{calc}/g cm^{-3}	1.426	1.506	1.586
μ/mm^{-1}	0.444	0.511	0.628
F(000)	546	492	1048
Data/restraints/parameters	5834/3/673	4712/3/305	3795/0/309
Goodness-of-fit on F^2	0.971	1.012	1.091
R indices, [$I > 2\sigma(I)$] R_1, wR_2	0.0621, 0.1198	0.0441, 0.0985	0.0354, 0.0920
R indices (all data): R_1, wR_2	0.0856, 0.1349	0.0559, 0.1041	0.0411, 0.0967
Residual electron density (e Å^{-3})	0.368, −0.378	0.782, −0.395	0.348, −0.385

2.7 DFT calculations

The geometries of compounds **1–8** were optimized in the gas phase with the Gaussian 09 (revision B. 01) software[25] using the 6-31+G(d,p) basis set[26] and the B3LYP functional[27] for non-metallic atoms and the LANL2DZ[28] effective core potential for vanadium. Starting models were obtained from the crystal structures where possible or derived from them. TD-DFT calculations were also done using these basis sets.

2.8 Cytotoxicity assays

The cytotoxicities of these complexes were determined using a PromegaCellTiter 96® AQueous One Solution Cell Proliferation Assay kit (Cat # G3580) containing a tetrazolium complex following the manufacturer's instructions. Briefly, 10 000 HARA cells (human squamous cell lung carcinoma cell line), kindly provided by Dr Haruo Iguchi,[29] Clinical Research Institute, National Hospital Organization Shikoku Cancer Center, Matsuyama, Japan, were plated in 100 μL RPMI growth medium (supplemented with 10% fetal bovine serum and penicillin–streptomycin) per well in 96 well plates. After overnight incubation at 37 °C in a CO_2 incubator with 5% CO_2, the complexes were added to cells at various concentrations with 200 μL serum-free growth medium per well. Each concentration was used in duplicate wells. All the complexes were dissolved in 100% DMSO and diluted in the growth media to provide various concentrations. After 72 h incubation, the medium was carefully aspirated from the wells and 100 μL serum-free colourless growth medium was added to each well. Then, 20 μL of CellTiter 96 AQueous One Solution Reagent was added into each well of the 96-well assay plate. After 1 hour incubation at 37 °C in a CO_2 incubator, the amount of soluble formazan was determined by absorbance at 450 nm. As NADPH or NADH, produced by dehydrogenase enzymes in metabolically active cells, reduces an MTS tetrazolium compound to a coloured formazan product that is soluble in tissue culture medium,[30,31] the amount of formazan produced is directly proportional to the number of living cells in culture. Viability is measured by the number of viable cells (percent of untreated control cells) for each concentration, expressed as the percent of viable cells in untreated control wells, which was arbitrarily assigned 100% viability, and represented as the standard error of the mean (SEM) of the triplicate wells for each concentration used in this assay.

2.9 Method of nuclear staining for apoptosis assay

We used a microscopic method to detect apoptotic nuclei using a nucleic acid staining dye, 4,6-diamidino-2-phenylindole (DAPI). We followed the procedure as described by Dash *et al.*,[32] in which HARA cells were plated on glass chamber slides (Lab-TekII Chamber slides, Nunc) and then grown for 24 hours before being treated with these complexes or left untreated (non-apoptotic control). After 48 hours of treatment, cells were fixed with 3.7% formaldehyde for 15 minutes. Subsequently, they were washed three times with 1× phosphate buffered saline (PBS), permeabilized with 0.1% Triton X-100 and stained with 1 μg ml^{-1} DAPI (prepared in 1× PBS) for 5 minutes at 37 °C. After the DAPI solution was aspirated, cells were washed three times with 1× PBS, mounted with mounting medium, which held cover slips in place and examined by fluorescence microscopy using a Leica DM IL LED microscope at a 40× objective.

2.10 Method for molecular docking studies

The DFT optimized structures of complexes **1–8** were used in docking. The coordinates of the Bcl-2 protein (PDB: 4LVT) were obtained from the Protein Data Bank for docking studies. Molecular docking studies for these complexes were carried out using AutoDock 4.2.[33] In these studies, the conformations of the complexes were allowed to change but that of the Bcl-2 protein was fixed. The data obtained from docking were examined with the PyMOL (http://pymol.sourceforget.net/) software.[34] Discovery Studio 4.1 Client and Chimera 1.10.1rc were used for visualization effects.

2.11 Method for antimicrobial activity

Staphylococcus aureus MTCC Code 96, *Bacillus subtilis* MTCC Code 736, *Salmonella typhimurium* MTCC Code 98 and *Escherichia coli* MTCC Code 68 were obtained from MTCC, Institute of Microbial Technology, Chandigarh, India. Antibacterial effects were assessed by microdilution methods.[35] Briefly, the four investigating bacteria were cultured overnight in nutrient broth and the cell densities were estimated at 1×10^5 CFUs ml^{-1} separately. Reactions were performed in a 96 well plate consisting of standard commercially available nutrient broth (NB) which was obtained from HIMEDIA (200 μL), inoculum (20 μL) and different dilutions of test samples. Following 24 h incubation at 37 °C, 40 μL (0.2 mg ml^{-1}) iodonitrotetrazolium chloride (INT) was added to each well and incubated for another 30 min. Each set was done in triplicate. IC_{50}, the concentration at which 50% growth of bacteria is inhibited in comparison with positive control, was calculated from the calibration curve prepared using percentages of inhibition against concentrations in μM. Streptomycin was used as a standard drug.

3. Results and discussion

3.1 Synthesis

The mixed-ligand oxidovanadium(IV) complexes $[V^{IV}O(L^{1-4})(phen)]$ (**1–4**) and oxidovanadium(V) complexes $[V^{V}O(L^{1-4})(hq)]$ (**5–8**) incorporating 1,10-phenanthroline (phen) and 8-hydroxyquinoline (Hhq), respectively, as auxiliary ligands have been prepared by the reaction of $[V^{IV}O(aa)_2]$ with equimolar amounts of the respective H_2L (where H_2L represents the general abbreviation of H_2L^{1-4}) followed by addition of equivalent amounts of the respective auxiliary ligands in methanol under aerobic conditions. The aerial dioxygen most likely acts as an oxidizing agent for the formation of the +V state of vanadium in complexes **5–8**. The formation reactions may be represented by the following eqn (1) and (2):

$$[V^{IV}O(aa)_2] + H_2L + phen \rightarrow [V^{IV}O(L)(phen)] + 2Haa \quad (1)$$

$$2[V^{IV}O(aa)_2] + 2H_2L + 2Hhq + 1/2O_2 \rightarrow 2[V^{V}O(L)(hq)] + 4Haa + H_2O \quad (2)$$

3.2 Description of the crystal structures

3.2.1 Description of the structure of 2. Crystals of complex **2** belong to the triclinic crystal system, in the non-centrosymmetric space group *P*1, in which the asymmetric unit consists of two molecules (Fig. S1, ESI†), called **A** and **B**, which have similar geometries and closely matching dimensions. For clarity, only molecule **A** is shown in Fig. 1. Each molecule is composed of a central vanadium ion in a distorted octahedral environment surrounded by one tridentate dinegative hydrazone ligand bound in a meridional manner (*mer*-ONO donor set in the enol form), one symmetrical bidentate neutral 1,10-phenanthroline (phen; N,N donor set) spanning equatorial and axial positions along with an oxido ion at the other axial position, indicating the +IV oxidation state of vanadium (also confirmed by magnetic susceptibility measurements and EPR spectral analysis, *vide infra*). Selected bond lengths and bond angles in the metal coordination spheres of **A** and **B** molecules are compared in Table 2. There are also two other potential donor sites in the coordinated hydrazone ligand, *viz.*, amine-N3 and the other imine-N2 which are not coordinated due to non-planarity with the former three donor sites. However, in both molecules, the two hydrogen atoms of amine-N3 form donor hydrogen bonds, intermolecular to N2 and intramolecular to O1 with the dimensions listed in Table 3. In the distorted octahedral environment around the metal, one phenolic-O, O1, one amide-O, O2 (in the enol form), and one imine-N, N1, of the doubly deprotonated meridionally disposed $(L^2)^{2-}$ ligand along with one of the two pyridine nitrogens N5 of the phen ligand constitute the equatorial plane with r.m.s. deviations of 0.007 and 0.002 Å from which the vanadium atom is displaced by 0.384(4) and 0.388(3) Å towards the axial terminal O3 in molecules **A** and **B** respectively. The second axial position is occupied by the other pyridine nitrogen N4 of phen, thus binding this symmetrical ligand to metal asymmetrically. This hydrazone ligand generates a six-membered ring and a five-membered chelate ring at the vanadium center, with the corresponding bite angles being 86.2(3)° and 78.2(3)° for **A** and 85.9(3)° and 78.1(3)° for **B** respectively. The atoms in the five-membered ring are closely coplanar with r.m.s. deviations of 0.010 and 0.013 Å, respectively, for **A** and **B**, while the six-membered ring is folded. The C–O, C–N and N–N bond lengths in the five-membered chelate ring are consistent with the enolate form of the amide. The atoms in the third chelate ring, [V1–N4–C27–C28–N5], formed by phen are also approximately coplanar (with r.m.s. deviations of 0.027 and 0.009 Å) with bite angles of 73.1(3)° and 73.3(3)°, respectively, and this plane is almost perpendicular to the equatorial plane intersecting at angles 88.9(2)° and 89.7(2)° respectively. The shortest and longest bonds formed by the metal atom are the two axial bonds formed by the terminal oxido group V≡O3 and the axial-N (V–N4), with the latter being lengthened due to the *trans* influence of the oxido atom. It is to be noted that such type of asymmetric binding of the phen ligand is also observed with other ONO donor ligand environments.[36] The three vanadium–oxygen bond lengths in the complex follow the order: oxido < phenolato < amide, which is probably due to the order of O → V π-bonding.

Table 2 Selected bond lengths (Å) and bond angles (°) in complex **2**

Complex	2A	2B
Bond lengths, Å		
V–O1	1.942(6)	1.947(6)
V–O2	1.971(6)	1.991(6)
V–O3	1.606(7)	1.607(6)
V–N1	2.067(8)	2.070(7)
V–N4	2.251(8)	2.322(8)
V–N5	2.118(7)	2.136(7)
Bond angles, deg		
O3–V–O2	102.4(3)	101.0(3)
O3–V–O1	101.0(3)	102.9(3)
O3–V–N4	167.2(3)	168.1(3)
O3–V–N5	94.1(3)	94.8(3)
O3–V–N1	107.5(3)	106.3(3)
O2–V–N4	79.5(3)	79.2(3)
O2–V–N5	90.0(3)	92.2(3)
O2–V–N1	78.2(3)	78.1(3)
O1–V–O2	154.9(3)	154.2(2)
O1–V–N4	79.8(2)	79.5(3)
O1–V–N5	97.3(3)	95.4(3)
O1–V–N1	86.2(3)	85.9(3)
N5–V–N4	73.1(3)	73.3(3)
N1–V–N4	85.3(3)	85.5(3)
N1–V–N5	157.0(3)	158.1(3)

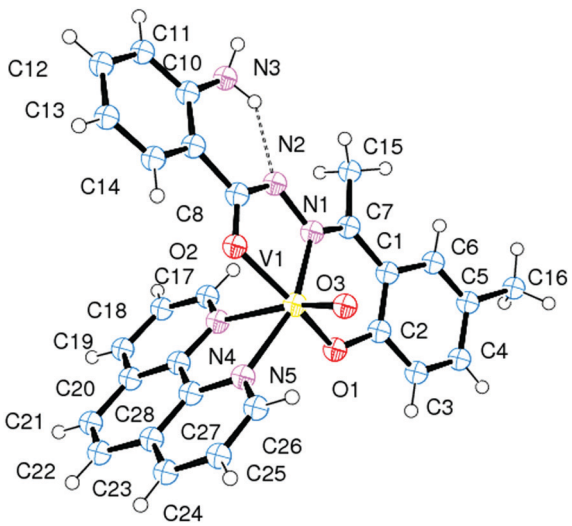

Fig. 1 Molecular structure of **2**, molecule **A**, with ellipsoids at 30% probability. The structure of molecule **B** is equivalent. The intramolecular hydrogen bond is shown as a dotted line.

3.2.2 Description of the structures of 5 and 8. Crystals of complex **5** belong to the triclinic system with space group $P\bar{1}$, while complex **8** belongs to the monoclinic crystal system with the $P2_1/n$ space group. The molecular structures of **5** and **8** are displayed in Fig. 2 and 3 respectively.

Like complex **2**, complexes **5** and **8** also consist of a neutral unit composed of a central vanadium ion in a distorted octahedral environment surrounded by one tridentate dinegative hydrazone ligand bound in a meridional manner (*mer*-ONO donor set in the enol form), one bidentate mononegative 8-hydroxyquinoline (hq^-; O^-,N donor set, in contrast to **2**,

Table 3 Dimensions of hydrogen bonds (distances, Å, angles (deg)) in complex **2**

D–H···A	*d*(D–H)	*d*(H···A)	*d*(D···A)	∠(DHA)	Symmetry element
N3A–HN3A···N2A	0.86(2)	1.99(5)	2.684(10)	136(6)	
N3A–HN3B···O1B	0.87(2)	2.44(7)	2.994(9)	122(7)	$1 + x, y - 1, z - 1$
N3B–HN3C···O1A	0.86(2)	2.12(3)	2.952(10)	164(7)	
N3B–HN3D···N2B	0.86(2)	2.00(5)	2.664(10)	133(6)	

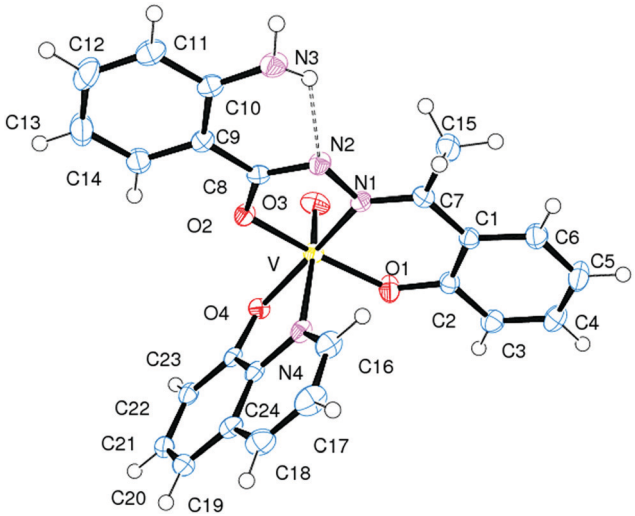

Fig. 2 Molecular structure of **5** with ellipsoids at 30% probability. The intramolecular hydrogen bond is shown as a dotted line.

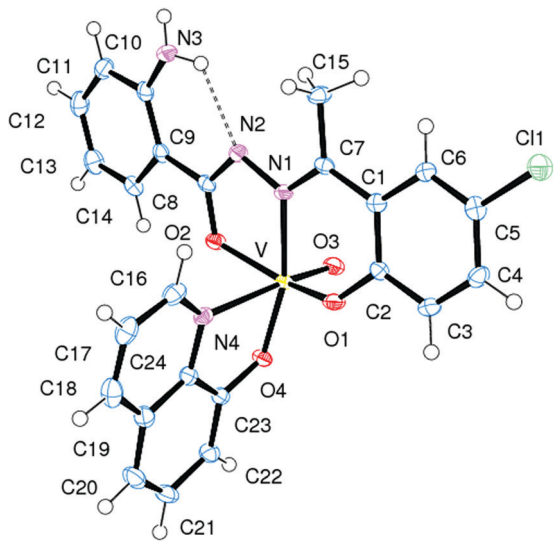

Fig. 3 Molecular structure of **8** with ellipsoids at 30% probability. The intramolecular hydrogen bond is shown as a dotted line.

which contains a neutral bidentate N,N donor set) spanning equatorial and axial positions along with an oxido ion at the other axial position indicating the +V oxidation state (*cf.* the +IV oxidation state in **2**) of vanadium (also confirmed by magnetic susceptibility measurements, *vide infra*). Selected bond-lengths and bond angles in the two metal coordination spheres are compared in Table 4. The remaining two potential donor sites

Table 4 Selected bond lengths (Å) and angles (°) in complexes **5** and **8**

Complex	**5**	**8**
Bond lengths, Å		
V–O1	1.8212(16)	1.8281(17)
V–O2	1.9316(15)	1.9338(16)
V–O3	1.6015(16)	1.5896(16)
V–O4	1.8508(14)	1.8536(15)
V–N1	2.1077(17)	2.099(2)
V–N4	2.3235(18)	2.383(2)
Bond angles, deg		
O3–V–O1	99.69(8)	101.48(8)
O3–V–O4	98.99(7)	98.40(7)
O1–V–O4	103.88(7)	101.81(7)
O3–V–O2	97.44(7)	98.64(8)
O1–V–O2	155.29(7)	152.07(7)
O4–V–O2	90.80(6)	94.14(7)
O3–V–N1	100.83(7)	95.64(8)
O1–V–N1	83.74(7)	83.15(7)
O4–V–N1	157.23(7)	163.81(7)
O2–V–N1	75.63(6)	75.75(7)
O3–V–N4	174.86(8)	173.87(8)
O1–V–N4	83.96(7)	80.51(7)
O4–V–N4	76.53(6)	75.49(6)
O2–V–N4	80.24(6)	81.51(7)
N1–V–N4	83.11(6)	90.35(7)

(*viz.*, the amine-N3 and the other imine-N2) which are non-planar to the bonded three donor sites are not bonded to the metal. However, in **5**, N3 forms two donor hydrogen bonds; one is intramolecular to N2 and the other is intermolecular to the terminal oxygen O3($1 - x$, $1 - y$, $-z$), thus forming a centro-symmetric dimer. A similar arrangement is found in **8** with an intramolecular hydrogen bond to N2 and an intermolecular hydrogen bond to O3($2 - x$, $-y$, $-z$). It will be noted that in **8**, unlike in **5**, the same hydrogen atom is involved in both bonds, with the second hydrogen not involved. The detailed dimensions of these H-bonds are given in Table 5. In both structures, the vanadium atom is bonded to four oxygen atoms and two nitrogen atoms to form a distorted octahedral geometry. One phenolate O1, one amide O2 (in the enol form) and the imine nitrogen N1 of the doubly deprotonated meridionally disposed $(L)^{2-}$ ligand along with the phenolic oxygen O4 of the deprotonated 8-hydroxyquinoline (hq^-) constitute the equatorial plane with r.m.s. deviations of 0.035 and 0.045 Å, from which the vanadium atom is displaced by 0.307(1) and 0.288(1) Å towards the terminal O3 atom in the two structures respectively. The second axial position is occupied by the pyridine nitrogen N4 of hq^-. These hydrazone ligands generate a six-membered ring and a five-membered chelate ring at the vanadium centre, with the corresponding bite angles being 75.63(6) and 75.76(7)° in **5** and **8** respectively. The atoms in the five-membered ring are closely coplanar with r.m.s. deviations of 0.042 and 0.023 Å,

Table 5 Dimensions of hydrogen bonds (distances, Å; angles (deg)) in **5** and **8**

D–H···A	d(D–H)	d(H···A)	d(D···A)	∠(DHA)	Symmetry element
5					
N3–H3A···O3	0.84(2)	2.20(2)	3.019(2)	165(2)	$1-x, 1-y, -z$
N3–H3B···N2	0.86(2)	2.09(2)	2.702(3)	128(2)	
8					
N3–HN3B···N2	0.83(2)	2.12(2)	2.725(3)	130(2)	
N3–HN3B···O3	0.83(2)	2.47(2)	2.941(3)	117(2)	$2-x, -y, -z$

respectively, while the six-membered ring is folded. The C–O, C–N, and N–N bond lengths of the five-membered chelate ring are consistent with the enolate form of the amide. The atoms in the third chelate ring formed by the hq^- are also approximately coplanar (with r.m.s. deviations of 0.043 and 0.021 Å) with bite angles of 76.53(6) and 75.49(6)°, respectively, and this plane is almost perpendicular to the equatorial plane intersecting at angles of 86.05(5) and 88.22(4)° in **5** and **8** respectively. As in complex **2**, the shortest and longest bonds are formed by the two axial atoms the terminal oxido group [*i.e.*, V≡O3] and V–N4, which is lengthened due to the *trans* influence of the oxido atom. The V≡O3 (oxido), V–O1 (phenolato) and V–O2 (amido/enolato) bond lengths are well within the range reported for VO^{3+} complexes, with carbonic acid hydrazide ligands and hq^- co-ligands.[11a,f,g,j,k] As a consequence of O → V π-bonding, these four vanadium–oxygen bond lengths in the complexes are in the order: oxido < phenolato < amide. However, as expected, the two phenolate bonds, namely, V–O1 [1.8212(16) in **5**; 1.8281(17) in **8**] and V-O4 [1.8508(14) in **5**; 1.8536(15) in **8**], are not similar.

3.3 IR spectra of the complexes

The characteristic ligand bands in the regions 1628–1668, 2918–3059 and 3444–3477 cm^{-1} due to C=O, N–H and O–H stretches, respectively, are not observed in their corresponding vanadium complexes, indicating the transformation of the C=O and N–H groups to the enolic form and their subsequent coordination to vanadium through the deprotonation of the phenolic and enolic hydrogens. A new band appearing in the 1244–1262 cm^{-1} region in the complexes was assigned to the C–O (enolate) mode. The strong band near 1565–1597 cm^{-1} is attributed to the C=N bond, while the V≡O stretching bands are observed in the 954–968 cm^{-1} region, indicating a hexa-coordinated environment around the metal centre.[11,15–17] The N–N band was observed in the 1013–1044 cm^{-1} region, indicating a 109–122 cm^{-1} shift to a higher wave number upon complexation due to the diminished repulsion between the lone pairs of adjacent nitrogen atoms. A sharp band observed in the 3085–3445 cm^{-1} region is likely to be associated with the intramolecularly H-bonded phenolic O–H group.

3.4 UV-Visible spectra of the complexes

Electronic spectra of complexes **1–8** were recorded in CH_2Cl_2 solution. The tetravalent complexes **1–4** display two ligand-field transitions in the near IR-visible region: one near 840–864 nm and other around the 720–774 nm region (Table 6) due to the $d_{xy} \rightarrow d_{xz,yz}$ and $d_{xy} \rightarrow d_{x^2-y^2}$ transitions respectively.[3b] The expected third transition due to the $d_{xy} \rightarrow d_{z^2}$ transition is probably masked by the strong charge transfer band at higher energies. The strong absorption at around 406–418 nm may be due to the charge transfer of the type O(phenolic) → V^{4+}. The intra-ligand π → π* transition (of the C=N bond) is observed near 320 nm (Fig. S2, ESI†). Complexes **5–8** display two intense transitions in the 300–800 nm region: one in the 536–550 nm region (Fig. S3, ESI†) and the other in the 329–332 nm region. These transitions arise due to the ligand to metal charge transfer (LMCT) transitions and the intra-ligand π → π* transition (of the C=N bond) respectively. The LMCT transitions are expected as they are observed in similar types of complexes.[11]

For complexes **5–8**, the λ_{max} values for the LMCT transitions exhibited a linear relationship (eqn (3)) (Fig. 4) with the Hammett parameter (σ) value of the substituents with an r value of 1.00.

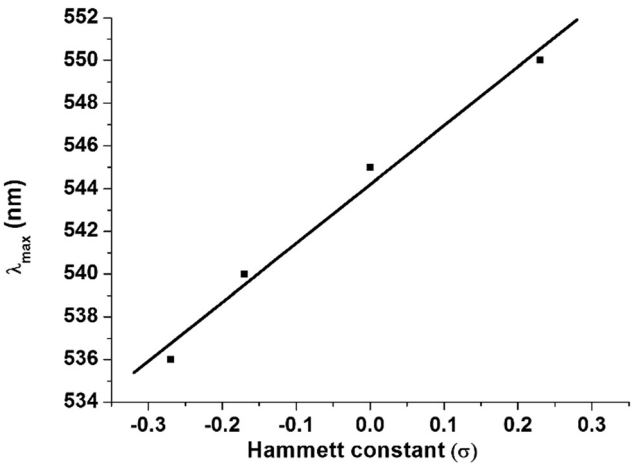

Fig. 4 Plot of λ_{max} *versus* the Hammett constant (σ) for complexes **5–8**.

Table 6 Electronic spectral and electrochemical data at 298 K of complexes **1–8** in CH_2Cl_2 solution

Complex	λ_{max}, nm (ε, $dm^3\ M^{-1}\ cm^{-1}$)	$E_{1/2}$ (V) (ΔE) (mV)
$[V^{IV}O(L^1)(phen)]$ (**1**)	851 (40), 755 (40), 410 (12 380), 321 (12 230)	0.65 (330)
$[V^{IV}O(L^2)(phen)]$ (**2**)	842 (30), 774 (30), 409 (13 630), 322 (15 720)	0.62 (360)
$[V^{IV}O(L^3)(phen)]$ (**3**)	840 (30), 724 (30), 406 (8530), 322 (16 670)	0.59 (500)
$[V^{IV}O(L^4)(phen)]$ (**4**)	864 (40), 720 (30), 418 (17 510), 324 (16 920)	0.71 (220)
$[V^{V}O(L^1)(hq)]$ (**5**)	545 (4320), 329 (9490)	−0.16 (120)
$[V^{V}O(L^2)(hq)]$ (**6**)	540 (8940), 330 (20 820)	−0.18 (120)
$[V^{V}O(L^3)(hq)]$ (**7**)	536 (11 140), 329 (30 830)	−0.19 (184)
$[V^{V}O(L^4)(hq)]$ (**8**)	550 (6420), 332 (16 200)	−0.14 (250)

The relationship indicates that the dependence of the λ_{max} value on the substituent is 27.55 nm.

$$\text{UV-vis: } \lambda_{max}\ (\text{nm}) = 544.19 + 27.55 \times \sigma \qquad (3)$$

3.5 Electrochemical properties of the complexes

The electrochemical properties of complexes **1–8** were examined in CH_2Cl_2 solution (0.1 M TBAHP) by cyclic voltammetry using a Pt working electrode, a Pt auxiliary electrode and a Ag/AgCl reference electrode and are listed in Table 6. The tetravalent complexes **1–4** exhibit quasi-reversible one electron oxidation peaks in the 0.59 to 0.71 V region, while the pentavalent complexes **5–8** display quasi-reversible one-electron reduction peaks in the −0.14 to −0.19 V region. Representative spectra of complexes **1** and **8** are displayed in Fig. 5 and 6 respectively. Analysis of the $E_{1/2}$ values of these two set of complexes indicates that they decrease with the increasing electron donating property of *para* substituents and the reverse is true for electron withdrawing substituents. Plots of the $E_{1/2}$ values of complexes **1–4** and **5–8** *versus* the σ values of the respective substituents give the following linear relationships (eqn (4) and (5) respectively, Fig. 7 and 8) with an r value of 1.0.

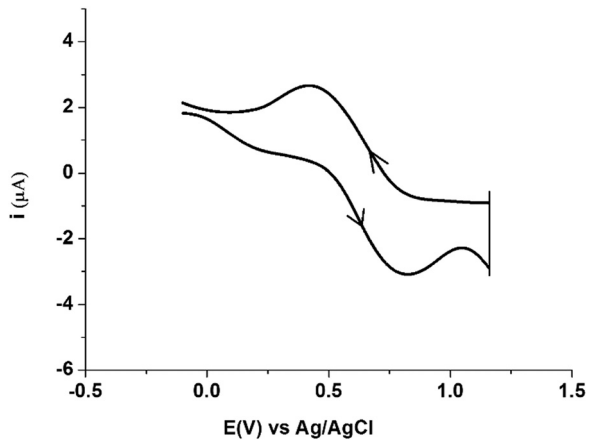

Fig. 5 Cyclic voltammogram of complex **1** in CH_2Cl_2 solution.

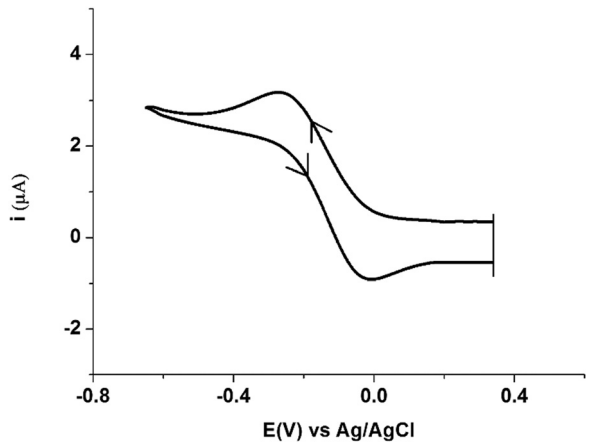

Fig. 6 Cyclic voltammogram of complex **8** in CH_2Cl_2 solution.

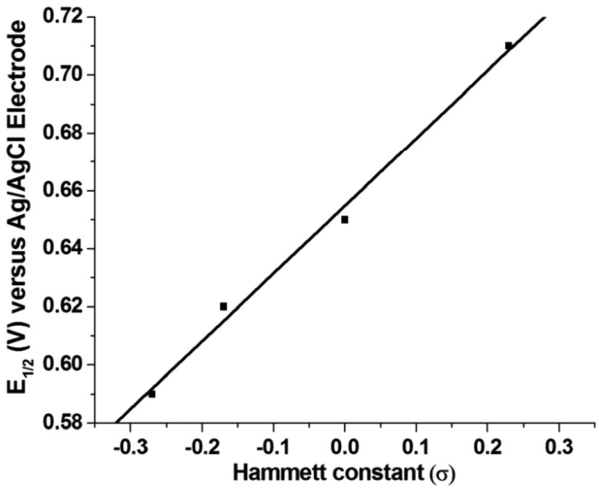

Fig. 7 Plot of $E_{1/2}$ *versus* the Hammett constant (σ) for complexes **1–4**.

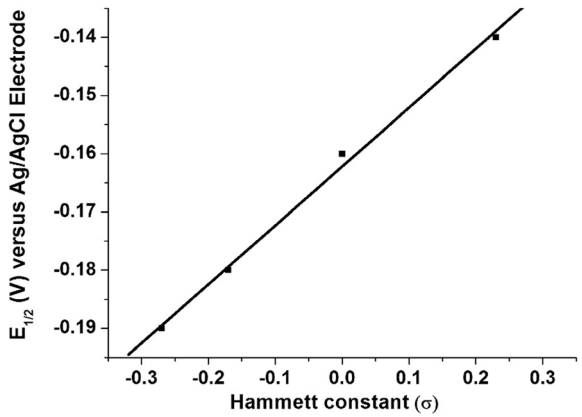

Fig. 8 Plot of $E_{1/2}$ *versus* the Hammett constant (σ) for complexes **5–8**.

$$\text{CV: } E_{1/2}\ (\text{V}) = 0.654 + 0.23 \times \sigma \qquad (4)$$

$$\text{CV: } E_{1/2}\ (\text{V}) = -0.162 + 0.10 \times \sigma \qquad (5)$$

3.6 ^{1}H NMR spectra of the ligands and complexes 5–8

The ^{1}H NMR spectra of the ligands were recorded in DMSO-d_6 solvent, while those of complexes **5–8** were recorded in $CDCl_3$ solvent. The data are given in the Experimental section. The phenolic O–H group of the acetophenone moiety of the free hydrazone ligand exhibits resonance in the δ 12.63–13.23 ppm region. However, this signal is not observed in complexes **5–8**, suggesting that the phenolic OH group of the acetophenone moiety is involved in bonding to vanadium through deprotonation. All the aromatic protons of the complexes are observed in the δ 6.59–8.15 ppm region.

3.7 ^{51}V NMR spectra of complexes 5–8

Like the ^{1}H NMR spectra, the ^{51}V NMR spectra of the pentavalent complexes **5–8** (recorded in $CDCl_3$ solution at room temperature) may also be used to examine the stability of these pentavalent complexes in solution. The ^{51}V NMR spectra of these complexes are displayed in Fig. S4 (ESI†). One sharp signal is obtained in

each of the four complexes **5–8**, respectively, at −480.32, −475.76, −468.91 and −475.11 ppm, suggesting that these complexes are stable in solution.

3.8 Magnetic properties of the complexes

The magnetic susceptibilities of all the complexes were measured at room temperature. The data indicate that complexes **1–4** are paramagnetic [the effective magnetic moments (μ_{eff}) values are ~1.70 μ_B, Table 7], while the other complexes **5–8** are diamagnetic, suggesting the +IV (in **1–4**) and +V (in **5–8**) oxidation states of vanadium. The μ_{eff} values for complexes **1–4** are typical for one unpaired electron per formula unit, suggesting that these complexes are monomeric with very weak or no antiferromagnetic interactions between the V atoms of the neighbouring molecules.

3.9 EPR spectra of complexes 1–4

The X-band EPR spectra of the tetravalent complexes **1–4** were recorded in CH_2Cl_2 solution at 300 K and 77 K. The data are listed in Table 7 and a representative spectrum for **2** is shown in Fig. 9 and those for **1**, **3** and **4** are shown in Fig. S5–S7 (ESI†). At 300 K, a typical eight-line spectral pattern (Fig. 9a) is obtained with $g_{iso} \sim 2.00$ and $A_{iso} \sim 95 \times 10^{-4}$ cm^{-1}, and at 77 K, a well-resolved axial anisotropy with an 8-line hyperfine structure (Fig. 9b), characteristic of a mononuclear vanadium complex with nuclear spin (^{51}V, $I = 7/2$), is obtained. The spin-Hamiltonian parameters ($g_\parallel$, $g_\perp$, $A_\parallel$ and $A_\perp$) are comparable with similar types of V(IV) complexes having identical geometrical structures. The $g_\parallel < g_\perp$ and $A_\parallel \gg A_\perp$ relationships are characteristic of an axially compressed d^1_{xy} configuration.[11,15,37]

3.10 Computational study

The DFT optimized geometrical parameters of complexes **2**, **5** and **8** (Tables S1 and S2, ESI†) are in reasonable agreement with the values obtained from X-ray crystallographic data (Tables 2 and 4) and the DFT optimized structures of all the complexes are shown in Fig. 10. The MOs of selected frontier orbitals of the complexes in their ground state optimized geometries are shown in Fig. S8 (ESI†). The vertical excitation energies and oscillator strengths (*f*) of excited states obtained from TD-DFT calculations are given in Table 8. A comparison of the calculated data in Table 8 with the experimental data in Table 6 indicates that for the tetravalent complexes **1–4**, with the exception of the transition near 850 nm, all the other three observed transitions are predicted theoretically, while for the pentavalent complexes **5–8**, the observed two transitions are predicted by DFT calculations.

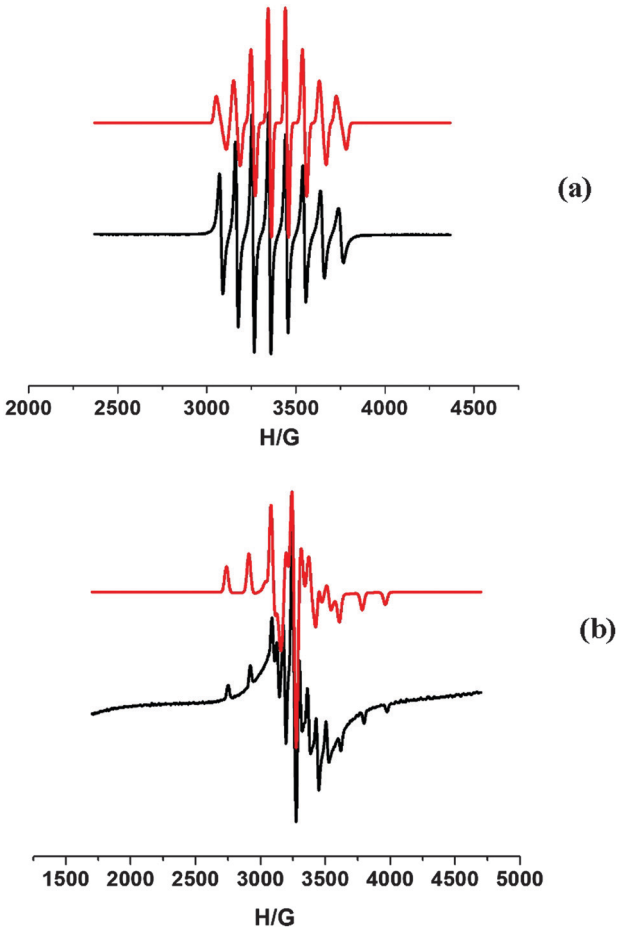

Fig. 9 X-band EPR spectra of complex **2** (black, experimental; red, simulated) in CH_2Cl_2 solution at (a) 300 K and (b) 77 K.

3.11 Study of cytotoxic activity of 1–8 complexes on lung cancer cell line

We tested the cytotoxic activity of these vanadium complexes on a lung cancer cell line (HARA cells) using cisplatin as a positive control. We chose the HARA cell line to test cytotoxicity because it is sensitive to metal complexes such as cisplatin and carboplatin which are used for the treatment of lung cancer. In this cytotoxicity assay, different complexes show a wide range of toxicities in a dose dependent manner (Fig. 11 and Table S3, ESI†). For example, in the series of mixed-ligand oxidovanadium(IV) complexes **1–4**, the IC_{50} values of complexes **2**, **3** and **4** are around 2.5 μM similar to that found for cisplatin, while that for complex **1** is 7.5 μM. In the case of mixed-ligand oxidovanadium(V) complexes **5–8**, the IC_{50} values of complexes **5**, **6** and **8** are *ca.* 12.5, 5 and 5 μM,

Table 7 μ_{eff} values at room temperature and EPR spectral parameters [*g* and *A* ($\times 10^{-4}$ cm^{-1})] of complexes **1–4** in CH_2Cl_2 solution at 300 K and 77 K

Complex	μ_{eff} (BM)	g_{iso}	A_{iso}	Line width (mT)	$g_\parallel$	$g_\perp$	g_{av}	$A_\parallel$	$A_\perp$	A_{av}	Line width (mT)
$[V^{IV}O(L^1)(phen)]$ (**1**)	1.65	1.978	94.55	1.8	1.95	1.99	1.977	171.27	57.12	95.17	2.3
$[V^{IV}O(L^2)(phen)]$ (**2**)	1.69	1.977	94.92	1.8	1.96	1.99	1.981	169.49	55.31	93.37	2.1
$[V^{IV}O(L^3)(phen)]$ (**3**)	1.68	1.978	94.20	1.8	1.95	1.99	1.977	170.92	55.32	93.85	2.0
$[V^{IV}O(L^4)(phen)]$ (**4**)	1.70	1.977	95.27	1.9	1.96	1.99	1.981	169.13	55.31	93.25	2.1

Limits of error in *g* values: ±0.01 and in *A* values: $\pm 3 \times 10^4$ cm^{-1}.

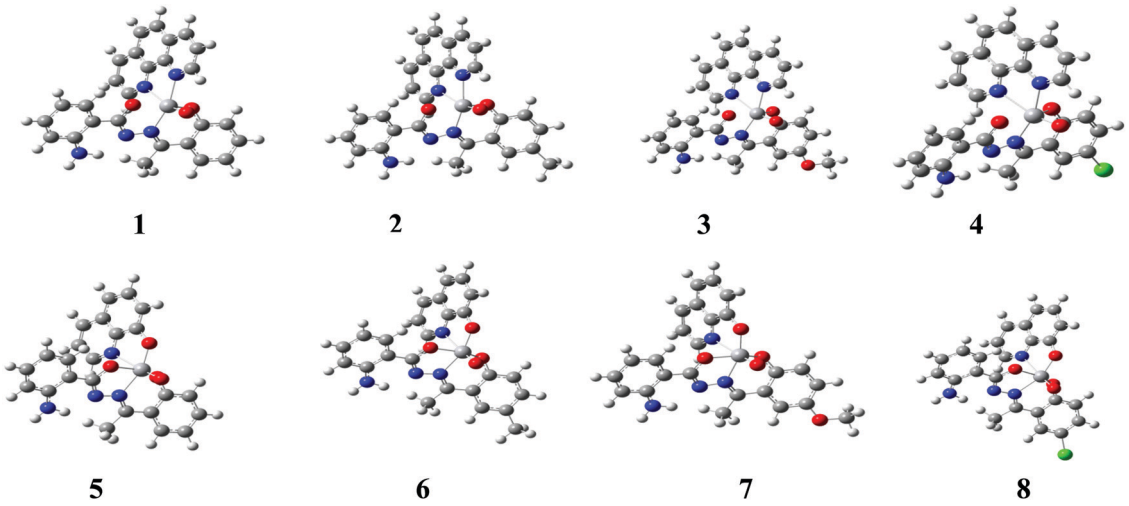

Fig. 10 DFT optimized structures of complexes **1–8**.

Table 8 Vertical excitation energies (E_{cal}), oscillator strengths (f_{cal}) and types of excitations of the excited states obtained from TD-DFT calculations of **1–8**

Complex	$E_{cal/nm}$	f_{cal}	Excitation
1	747.24	0.0006	HOMO → LUMO+2 (0.61233)
	419.60	0.1355	HOMO−2 → LUMO+2 (0.52862)
	354.37	0.0131	HOMO−2 → LUMO+3 (0.64620)
			HOMO−3 → LUMO+2 (0.81462)
2	750.18	0.0007	HOMO−1 → LUMO (0.65134)
	427.12	0.0847	HOMO−2 → LUMO+2 (0.53202)
	358.36	0.0155	HOMO−2 → LUMO+3 (0.64363)
			HOMO−2 → LUMO+1 (0.89699)
3	749.85	0.0007	HOMO−2 → LUMO+2 (0.49323)
	469.07	0.0723	HOMO−2 → LUMO+3 (0.62565)
	364.62	0.0149	HOMO → LUMO+1 (0.68691)
			HOMO → LUMO+4 (0.46513)
4	744.83	0.0007	HOMO−2 → LUMO+2 (0.42752)
	436.78	0.1820	HOMO−2 → LUMO+3 (0.67409)
	363.88	0.0123	HOMO → LUMO+1 (0.56039)
			HOMO−1 → LUMO (0.49992)
			HOMO−3 → LUMO (0.79485)
5	510.37	0.2442	HOMO−2 → LUMO (0.66657)
	341.46	0.0934	HOMO−3 → LUMO+2 (0.44942)
6	510.42	0.2290	HOMO−4 → LUMO (0.24404)
			HOMO−2 → LUMO (0.64910)
	346.65	0.0677	HOMO−3 → LUMO+2 (0.36927)
			HOMO−1 → LUMO+3 (0.41043)
7	517.21	0.1161	HOMO−3 → LUMO (0.50831)
			HOMO−2 → LUMO (0.46231)
	327.78	0.0423	HOMO−2 → LUMO+4 (0.63490)
8	513.5	0.2568	HOMO−2 → LUMO (0.68313)
	336.35	0.0423	HOMO−8 → LUMO (0.45235)
			HOMO−7 → LUMO (0.42766)

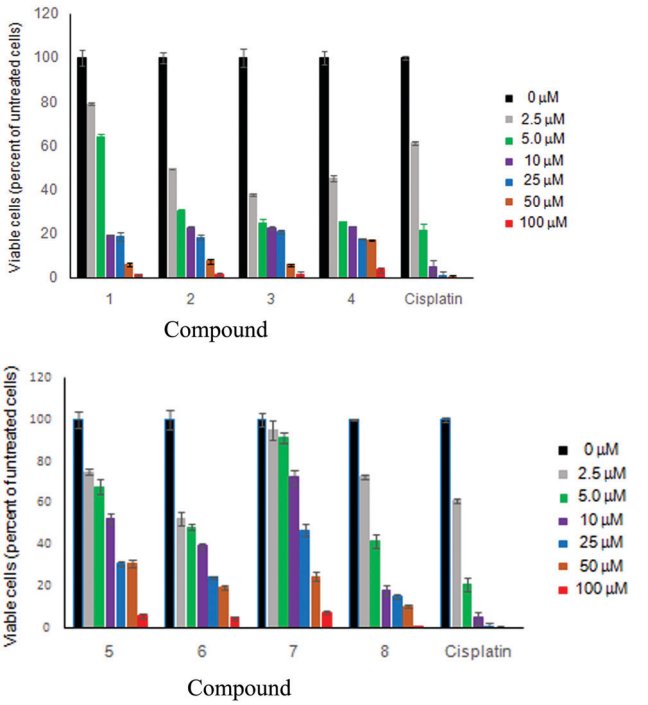

Fig. 11 Cytotoxic activity of complexes **1–8** and comparison with cisplatin.

respectively, while for complex **7** the value is 25 μM. It is noteworthy that the free H_2L^{1-4} ligands and $[V^{IV}O(aa)_2]$ show practically no toxicity (Fig. S9 and S10 respectively, ESI†), while the phen (IC_{50} ∼ 50 μM) and Hhq (IC_{50} ∼ 100 μM) ligands exhibit appreciably low toxicity (Fig. S11, ESI†) than all the complexes described here. It is to be noted that these complexes are stable under the experimental conditions as suggested by the spectral studies. It is noteworthy that in general these pentavalent complexes **5–8** are less toxic than the tetravalent complexes **1–4**. We also investigated the mechanism of cytotoxicity of these complexes using complexes **1** and **5** as representative samples (Fig. 12). We used nuclear staining of treated and untreated cells using DAPI, a DNA binding dye. Cells treated with complexes **1** and **5** show distinct chromatin condensation and fragmentation, a distinct characteristic of apoptosis. Fig. 12 shows the experimental proof of cell death treated with these complexes through apoptosis. Although complexes **1–4** belong to the same class of mixed-ligand oxidovanadium(IV) complexes, complexes **2–4** are potentially more toxic than complex **1**. Similarly, complexes **5–8** also

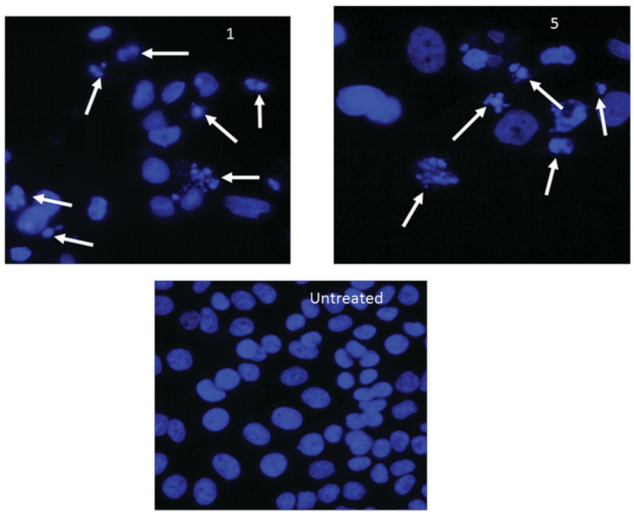

Fig. 12 Experimental proof of lung cancer cell death treated with complexes **1** and **5**.

belong to the same class of mixed-ligand oxidovanadium(v) complexes, but complexes **5**, **6** and **8** show potent toxicity, whereas complex **7** shows almost no toxicity in the concentration range used in this experiment. It is evident from this study that some of the complexes have the ability to kill lung cancer cells effectively, and in fact, complexes **2–4** are equally effective as cisplatin in killing human lung cancer cells and may be potential therapeutic candidates for the treatment of lung cancer.

3.12 Docking study

Simultaneous over-expression and under-expression of, respectively, anti-apoptotic and pro-apoptotic genes is the cause of cancer. The Bcl-2 protein is a result of expression of the anti-apoptotic gene.[38] Therefore, a high concentration of the Bcl-2 protein in cells decreases the levels of Bax and Bak proteins due to complex formation. This Bax protein is very important to cell apoptosis through the settlement of integrity of the external surfaces of mitochondria, which liberates pro-apoptotic signalling factors that can initiate the activation of caspase-9 and caspase-3 genes. So, blocking of the Bax binding site (BH3) [Fig. 13(a)] of the Bcl-2 protein by some small molecules frees Bax for apoptosis.

Molecular docking is a very important theoretical study used to find the binding site of a protein where a small molecule prefers to bind with the lowest energy.[39] To understand the mechanism of anti-lung cancer activity on HARA cells of the vanadium complexes, a docking study of all the vanadium complexes **1–8** with the Bcl-2 protein (PDB: 4LVT) has been done. The docking study shows that all the oxidovanadium(iv) complexes, namely $[V^{IV}O(L^{1-4})(phen)]$ (**1–4**), show greater activity than the oxidovanadium(v) complexes, namely $[V^{V}O(L^{1-4})(hq)]$ (**5–8**) as

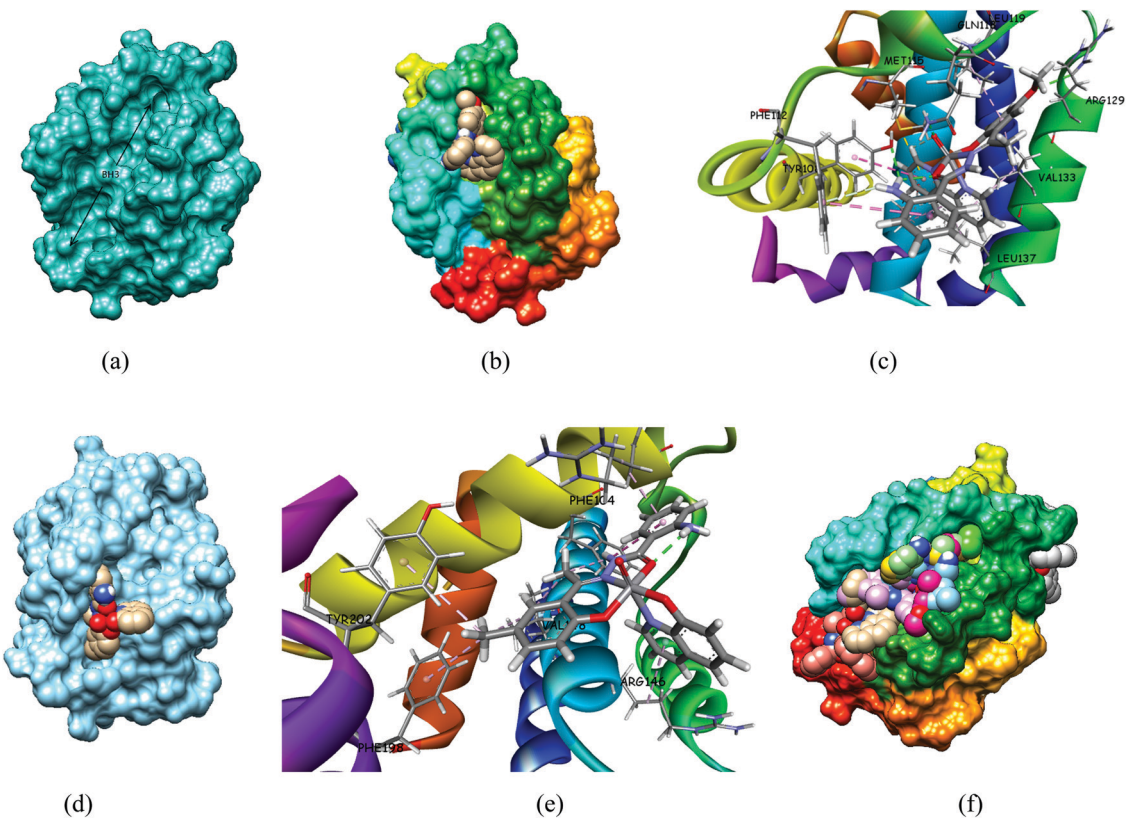

Fig. 13 (a) BH3 binding site of Bcl-2 protein, (b) binding site of compound **3**, (c) mode of interactions and amino acids of Bcl-2 interacting with **3**, (d) binding site of compound **6**, (e) mode of interactions of **6** with amino acids of Bcl-2, and (f) overlay of all the structures of complexes **1–8** inside the BH3 site.

shown in Table S3 (ESI†). In the docking study, compounds **3** and **6** were found to be best in their corresponding class in agreement with the experimental anticancer study. Compounds **2** and **4** also exhibit comparable binding energy with compound **3** and we found that complex **8** has a similar binding energy with the Bcl2 protein to complex **6** (Table S3 and Fig. S11c–e, ESI†). In fact, it is clear from Table S3 (ESI†) that the binding energies of the complexes with the Bcl-2 protein follow the experimental cytotoxicity order and the tetravalent complexes **2–4** are somewhat more toxic than the pentavalent complexes **5–8**. Two different pockets of the hydrophobic core of BH3 are the favoured binding sites of both the compounds [Fig. 13(b) and (d)]. Amino acid residues Tyr108, Phe112, Met115, Gln118, Leu119, Arg129, Val133, Leu137, and Ala194 are found in the vicinity of the bound compound **3**, whereas Arg146, Val148, Phe198, Ala100, Phe104, Arg107, and Tyr108 residues are present in the binding pocket for compound **8** [Fig. 13(c) and (e)]. Several non-covalent interactions including van der Waals interactions, hydrogen bonding, carbon hydrogen bonding, π-donor hydrogen bonding, π-sulphur, π–π staking, π–π T shaped and π-alkyl interactions are the binding forces for **3** [Fig. 13(c) and Fig. S12(a), ESI†]. However, van der Waals, π–π T shaped, π-alkyl and hydrophobic interactions play important roles for the binding of **6** [Fig. 13(e) and Fig. S12(b), ESI†]. It is interesting to note that all of these compounds prefer to bind at the BH3 binding site [Fig. 13(f)]. Therefore, these compounds effectively generate the signal of death and may initiate apoptosis by inhibiting the Bcl-2 from binding with Bax.

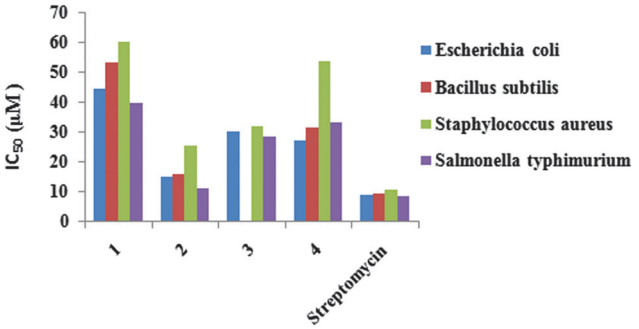

Fig. 14 Antimicrobial activity of complexes **1–4** and comparison with streptomycin.

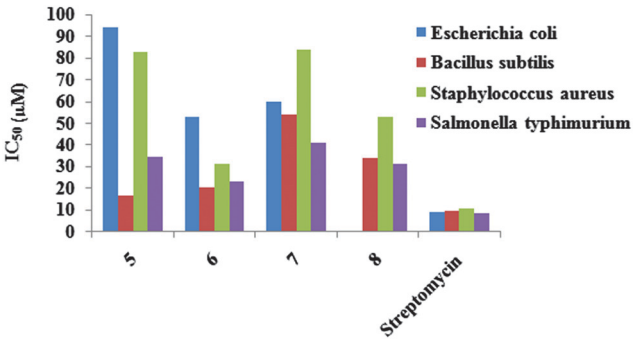

Fig. 15 Antimicrobial activity of complexes **5–8** and comparison with streptomycin.

3.13 Antimicrobial activity study

In this study, the synthesized complexes **1–8** along with the reference compound (streptomycin) and the ligands used in this study, namely, H_2L^{1-4}, phen and Hhq, were tested for *in vitro* antibacterial activity[40–43] against four pathogenic bacterial strains (Gram negative *Escherichia coli*, Gram positive *Bacillus subtilis*, Gram positive *Staphylococcus aureus* and Gram negative *Salmonella typhimurium*) by the microdilution method. The results listed in Table 9 show that almost all the test compounds (except for **3** for *Bacillus subtilis* and **8** for Gram negative *Escherichia coli*) showed good to excellent antibacterial activity (Fig. 14 and 15). The concentration of the stock solutions for all the complexes was 1 mM in 100% dimethyl sulfoxide (DMSO). Besides this, the dose–response curves for the antimicrobial activity of complexes **2** and **5** are shown in Fig. S12 and S13 (ESI†) respectively. For Gram negative *Escherichia coli*, the antibacterial activity follows the order: **2** > **4** > **3** > **1**, whereas for Gram positive *Staphylococcus aureus* and Gram negative *Salmonella typhimurium*, the antibacterial activity follows the order: **2** > **3** > **4** > **1**. For Gram positive *Bacillus subtilis*, the antibacterial activity follows the order: **2** > **4** > **1**, with **3** being inactive. Similarly, a scrutiny of the IC_{50} values indicates that

Table 9 IC_{50} values of complexes **1–8**, streptomycin (a standard drug) and the phen and Hhq ligands against *Escherichia coli*, *Bacillus subtilis*, *Staphylococcus aureus* and *Salmonella typhimurium*

	IC_{50} (μM) ± SD			
Complex	Gram negative *Escherichia coli*	Gram positive *Bacillus subtilis*	Gram positive *Staphylococcus aureus*	Gram negative *Salmonella typhimurium*
1	44.74 ± 1.49	53.5 ± 1.04	60.31 ± 1.09	39.88 ± 0.67
2	15.18 ± 1.56	16.09 ± 0.87	25.7 ± 0.76	11.2 ± 0.82
3	30.33 ± 0.49	—	32.17 ± 1.05	28.49 ± 0.49
4	27.37 ± 1.43	31.93 ± 0.49	53.83 ± 1.21	33.39 ± 1.01
5	94.14 ± 1.07	16.67 ± 1.65	82.63 ± 0.65	34.51 ± 0.79
6	52.84 ± 1.78	20.32 ± 1.08	31.5 ± 1.08	23.37 ± 0.68
7	60.03 ± 0.57	54.13 ± 0.98	83.66 ± 1.14	41.33 ± 1.07
8	—	34.17 ± 1.10	52.73 ± 0.48	31.25 ± 0.91
Streptomycin	9.3 ± 0.11	9.62 ± 0.009	10.81 ± 0.164	8.75 ± 0.02
phen	46.50 ± 1.89	63.88 ± 2.04	55.00 ± 1.17	103.27 ± 2.89
Hhq	63.51 ± 2.88	78.50 ± 1.69	62.50 ± 1.02	131.03 ± 2.13

complex **6** showed higher antimicrobial activity followed by **8**, **5** and **7** towards Gram positive *Staphylococcus aureus* and Gram negative *Salmonella typhimurium*. For Gram negative *Escherichia coli*, complex **8** is inactive, whereas **6** is the most active, and for Gram positive *Bacillus subtilis*, the order is: **5** > **6** > **8** > **7**. From the IC_{50} values of these complexes it is clear that most antimicrobial activity is found when the substituent at the *para* position in the aromatic ring is methyl. Among the eight complexes studied here, complex **2** exhibited excellent antibacterial activity as indicated by its low IC_{50} values ranging between 11.2 and 25.7 μM [whereas the IC_{50} values for streptomycin (standard drug) are 9.3 against *Escherichia coli*, 9.62 against *Bacillus subtilis*, 10.81 against *Staphylococcus aureus* and 8.75 against *Salmonella typhimurium*]. It should be noted that the H_2L^{1-4} ligands did not exhibit any such antibacterial activity even at high concentrations, whereas phen and Hhq displayed antibacterial activity against the above-mentioned four pathogenic bacteria. However, it is evident from the IC_{50} values (Table 9) that the phen and Hhq ligands are significantly less toxic than most of our reported complexes. It is also to be noted that DMSO did not affect the bacterial growth.

4. Conclusions

A family of 2-aminobenzoylhydrazone of 2-hydroxyacetophenone and its 5-substituted derivatives have been used as primary ligands, while 1,10-phenanthroline (phen) and 8-hydroxyquinoline (Hhq) have been used as auxiliary ligands in this work with a view to studying the effect of substituents on the electronic properties of the vanadium in the resulting complexes as well as on the oxidation state of vanadium. This study indicates that the auxiliary ligands have a remarkable effect on the selective stabilisation of a particular oxidation state of vanadium; for example, in the presence of the neutral bidentate N,N donor phen ligand, the +IV state of vanadium is stabilized in the mixed-ligand complexes, while the bidentate monoacidic O^-,N donor Hhq ligand stabilizes the +V state of vanadium. The complexes have been fully characterized by different spectroscopic techniques along with the structure determination of some of the reported complexes by X-ray diffractometry. In fact, to the best of our knowledge, the structure of complex **2** represents the first structural characterization of a mixed-ligand oxidovanadium(IV) complex containing tridentate ONO donor hydrazone as a primary ligand and a neutral bidentate N,N donor as an auxiliary ligand. The $E_{1/2}$ values of complexes **1–8** and the λ_{max} values for the LMCT transition of complexes **5–8** exhibited linear relationships with the Hammett parameter of the substituent. Some of the complexes exhibited promising anticancer activity comparable to that of cisplatin against lung cancer cell lines. It is noteworthy that the tetravalent complexes are more active than the pentavalent complexes. Furthermore, the substituents also have significant effects on their activity. These complexes also exhibited promising antimicrobial activity against four pathogenic bacterial stains, namely, *Escherichia coli*, *Bacillus subtilis, Staphylococcus aureus* and *Salmonella typhimurium*.

Conflicts of interest

There are no conflicts to declare.

Acknowledgements

We thank the University Grants Commission (New Delhi, India) for financial assistance (F.PSW-172/09-10). We are thankful to our College authority for providing research facilities. We gratefully acknowledge DST-FIST for instrumental help at the Ramakrishna Mission Vivekananda Centenary College, Rahara. We also thank EPSRC and the University of Reading for funds for the X-Calibur system. We are also grateful to Dr Ayan Datta, Department of Spectroscopy, Indian Association for the Cultivation of Science, Jadavpur, Kolkata, India, for his support in DFT calculation. We also thank Dr P. Ghosh, Ramakrishna Mission Residential College, Narendrapur, Kolkata, India, for instrumental help for electrochemical study. S. B. (PDF/2016/001935) is thankful to SERB, India, for the fellowships.

References

1 (*a*) D. Rehder, *Bioinorganic Vanadium Chemistry*, John Wiley & Sons Ltd., Chichester, UK, 2008; (*b*) D. Rehder, *J. Inorg. Biochem.*, 2000, **80**, 133–136.
2 S. Kundu, D. Mondal, K. Bhattacharya, A. Endo, E. Garribba and M. Chaudhury, *Inorg. Chem.*, 2015, **54**, 6203–6215.
3 (*a*) J. R. Winkler and H. B. Gray, *Struct. Bonding*, 2012, **142**, 17–28; (*b*) C. J. Ballhausen and H. B. Gray, *Inorg. Chem.*, 1962, **1**, 111–122.
4 (*a*) E. J. Baran, *Adv. Plant Physiol.*, 2008, **10**, 357–372; (*b*) M. Anke, *Anales de la Real Academia Nacional de Farmacia*, 2004, **70**, 961–999; (*c*) H. U. Meisch and H. J. Bielig, *Basic Res. Cardiol.*, 1980, **75**, 413–417.
5 (*a*) D. Rehder, G. Santonin, G. M. Licini, C. Schulzke and B. Meier, *Coord. Chem. Rev.*, 2003, **237**, 53–63; (*b*) W. Plass, *Coord. Chem. Rev.*, 2003, **237**, 205–212; (*c*) K. H. Thompson and C. Orvig, *Coord. Chem. Rev.*, 2001, **219**, 1033–1053; (*d*) A. Butler, *Coord. Chem. Rev.*, 1999, **187**, 17–35.
6 D. C. Crans, J. J. Smee, E. Gaidamauskas and L. Yang, *Chem. Rev.*, 2004, **104**, 849–902.
7 (*a*) R. R. Eady, *Coord. Chem. Rev.*, 2003, **237**, 23–30; (*b*) J. J. R. Frausto da Silva and R. J. P. Williams, *The Biological Chemistry of the Elements*, Oxford University Press, Oxford, UK, 2nd edn, 2001; (*c*) W. Kaim and B. Schwederski, *Bioinorganic Chemistry: Inorganic Elements in the Chemistry of Life – An Introduction and Guide*, John Wiley & Sons: Chichester, UK, 1994, vol. 5.
8 (*a*) D. C. Crans, *J. Org. Chem.*, 2015, **80**, 11899–11915; (*b*) C. C. McLauchlan, B. J. Peters, G. R. Willsky and D. C. Crans, *Coord. Chem. Rev.*, 2015, **301-302**, 163–199; (*c*) H. Yasui, Y. Adachi, A. Katoh and H. Sakurai, *J. Biol. Inorg. Chem.*, 2007, **12**, 843–853; (*d*) Y. Shechter, I. Goldwaser, M. Mironchik, M. Fridkin and D. Gefel, *Coord. Chem. Rev.*, 2003, **237**, 3–11; (*e*) K. H. Thompson, B. D. Liboiron, Y. Sun, K. D. D. Bellman, V. Karunaratne, G. Rawji, J. Wheeler, K. Sutton, S. Bhanot,

S. B. C. Cassidy, J. H. McNeill, V. G. Yuen and C. Orvig, *J. Biol. Inorg. Chem.*, 2003, **8**, 66–74; (*f*) K. H. Thompson, J. H. McNeill and C. Orvig, *Chem. Rev.*, 1999, **99**, 2561–2571.

9 M. R. Maurya, S. Agarwal, C. Bader, M. Ebel and D. Rehder, *Dalton Trans.*, 2005, 537–544.

10 (*a*) D. Sanna, V. Ugone, G. Micera, P. Buglyó, L. Bíró and E. Garribba, *Dalton Trans.*, 2017, 8950–8967; (*b*) L. Reytman, O. Braitbard, J. Hochman and E. Y. Tshuva, *Inorg. Chem.*, 2016, **55**, 610–618; (*c*) S. Ramos, J. J. G. Moura and M. Aureliano, *Metallomics*, 2012, **4**, 16–22; (*d*) E. Cobbina, S. Mehtab, I. Correia, G. Goncalves, I. Tomaz, I. Cavaco, T. Jakusch, E. Enyedi, T. Kiss and J. C. Pessoa, *J. Mex. Chem. Soc.*, 2013, **57**, 180–191; (*e*) J. Benítez, L. Becco, I. Correia, S. M. Leal, H. Guiset, J. C. Pessoa, J. Lorenzo, S. Tanco, P. Escobar, V. Moreno, B. Garat and D. Gambino, *J. Inorg. Biochem.*, 2011, **105**, 303–312; (*f*) R. K. Narla, Y. D. Dong, O. J. Cruz, C. Navara and F. M. Uckun, *Clin. Cancer Res.*, 2000, **6**, 1546–1556.

11 (*a*) T. Ghosh, S. Bhattacharya, A. Das, G. Mukherjee and M. G. B. Drew, *Inorg. Chim. Acta*, 2005, **358**, 989–996; (*b*) T. Ghosh and B. Mondal, *J. Chem. Res.*, 2007, 407–410; (*c*) B. Mondal, T. Ghosh, M. Sutradhar, G. Mukherjee, M. G. B. Drew and T. Ghosh, *Polyhedron*, 2008, **27**, 2193–2201; (*d*) B. Mondal, M. G. B. Drew and T. Ghosh, *Inorg. Chim. Acta*, 2009, **362**, 3303–3308; (*e*) B. Mondal, M. G. B. Drew and T. Ghosh, *Inorg. Chim. Acta*, 2010, **363**, 2296–2306; (*f*) T. Ghosh, B. Mondal, M. Sutradhar, G. Mukherjee and M. G. B. Drew, *Inorg. Chim. Acta*, 2007, **360**, 1753–1761; (*g*) D. Patra, N. Biswas, B. Mondal, M. G. B. Drew and T. Ghosh, *Polyhedron*, 2012, **48**, 264–270; (*h*) B. Mondal, M. G. B. Drew, R. Banerjee and T. Ghosh, *Polyhedron*, 2008, **27**, 3197–3206; (*i*) D. Patra, N. Biswas, B. Mondal, P. Mitra, M. G. B. Drew and T. Ghosh, *RSC Adv.*, 2014, **4**, 22022–22034; (*j*) N. Biswas, D. Patra, B. Mondal, M. G. B. Drew and T. Ghosh, *J. Coord. Chem.*, 2015, **69**, 318–329; (*k*) D. Patra, N. Biswas, B. Kumari, P. Das, N. Sepay, S. Chatterjee, M. G. B. Drew and T. Ghosh, *RSC Adv.*, 2015, **5**, 92456–92472; (*l*) N. Biswas, D. Patra, B. Mondal, S. Bera, S. Acharya, A. K. Biswas, T. K. Mukhopadhyay, A. Pal, M. G. B. Drew and T. Ghosh, *Dalton Trans.*, 2017, **46**, 10963–10985; (*m*) D. Patra, S. Paul, I. Majumder, N. Sepay, S. Bera, R. Kundu, M. G. B. Drew and T. Ghosh, *Dalton Trans.*, 2017, **46**, 16276–16293.

12 L. H. A. Terra, M. C. Areias, I. Gaubeur and M. E. V. Suez-Iha, *Spectrosc. Lett.*, 1999, **32**, 257–271.

13 (*a*) Z. Cui, X. Yang, Y. Shi, H. Uzawa, J. Cui, H. Dohi and Y. Nishida, *Bioorg. Med. Chem. Lett.*, 2011, **21**, 7193–7196; (*b*) M. R. Maurya, S. Agarwal, M. Abid, A. Azam, C. Bader, M. Ebel and D. Rehder, *Dalton Trans.*, 2006, 937–947; (*c*) L. Savini, L. Chiasserini, V. Travagli, C. Pelleran and E. Novellino, *Eur. J. Med. Chem.*, 2004, **39**, 113–122.

14 (*a*) P. Dandawate, E. Khan, S. Padhye, H. Gaba, S. Sinha, J. Deshpande, S. K. Venkateswara, M. Khetmalas, A. Ahmad and F. H. Sarkar, *Bioorg. Med. Chem. Lett.*, 2012, **22**, 3104–3108; (*b*) F. F. Tian, J. H. Li, F. L. Jiang, X. L. Han, C. Xiang, Y. S. Ge, L. L. Li and Y. Liu, *RSC Adv.*, 2012, **2**, 501–513; (*c*) G. S. Hassan, H. H. Kardy, S. M. Abou-Seri, M. M. Ali and A. E. Mahmoud, *Bioorg. Med. Chem.*, 2011, **19**, 6808–6817; (*d*) K. Effenberger, S. Breyer and R. Schobert, *Eur. J. Med. Chem.*, 2010, **45**, 1947–1954; (*e*) C. D. Fan, H. Su, J. Zhao, B. X. Zhao, S. L. Zhang and J. Y. Miao, *J. Med. Chem.*, 2010, **45**, 1438–1446; (*f*) W. Y. Liu, H. Y. Li, B. X. Zhao, D. S. Shin, S. Lian and J. Y. Miao, *Carbohydr. Res.*, 2009, **344**, 1270–1275; (*g*) Y. Xia, C. D. Fan, B. X. Zhao, J. Zhao, D. S. Shin and J. Y. Miao, *Eur. J. Med. Chem.*, 2008, **43**, 2347–2353; (*h*) J. Easmon, G. Puerstinger, K. S. Thies, G. Heinisch and J. Hofmann, *J. Med. Chem.*, 2006, **49**, 6343–6350; (*i*) T. B. Chaston, R. N. Watts, J. Yuan and D. R. Richardson, *Clin. Cancer Res.*, 2004, **10**, 7365–7374; (*j*) A. C. Cunha, J. M. Figueiredo, L. M. Tributino, A. L. P. Miranda, H. C. Castro, R. B. Zingali, C. A. M. Fraga, C. B. V. Souza, V. F. Ferreira and E. Barreiro, *Bioorg. Med. Chem.*, 2003, **11**, 2051–2059; (*k*) L. R. Morgan, B. S. Jursic, C. L. Hooper, D. M. Neumann, K. Thangaraj and B. LeBlanc, *Bioorg. Med. Chem. Lett.*, 2002, **12**, 3407–3411; (*l*) G. Darnell and D. R. Richardson, *Blood*, 1999, **94**, 781–792; (*m*) D. R. Richardson, *Antimicrob. Agents Chemother.*, 1997, **41**, 2061–2063; (*n*) G. R. Braslawsky, M. A. Edson, W. Pearce, T. Kaneko and R. S. Greenfield, *Cancer Res.*, 1990, **50**, 6608–6614.

15 J. Chakravarty, S. Dutta, A. Dey and A. Chakravorty, *J. Chem. Soc., Dalton Trans.*, 1994, 557–561.

16 S. X. Liu and S. Gao, *Polyhedron*, 1994, **17**, 81–84.

17 S. Nica, M. Rudolph, H. Görls and W. Plass, *Inorg. Chim. Acta*, 2007, **360**, 1743–1752.

18 R. A. Rowe and M. M. Jones, *Inorg. Synth.*, 1957, **5**, 113–116.

19 N. Biswas, S. Bera, N. Sepay, A. Pal, T. Halder, S. Ray, S. Acharyya, A. K. Biswas, M. G. B. Drew and T. Ghosh, *New J. Chem.*, communicated.

20 S. Stoll and A. Schweiger, *J. Magn. Reson.*, 2006, **178**, 42–55.

21 CrysAlis, Oxford Diffraction Ltd., Abingdon, UK, 2006.

22 G. M. Sheldrick, SHELXS97, *Acta Crystallogr., Sect. A: Found. Adv.*, 2008, **64**, 112.

23 Abspack, Oxford Diffraction Ltd., Abingdon, UK, 2005.

24 G. M. Sheldrick, SHELXL, *Acta Crystallogr., Sect. C: Struct. Chem.*, 2015, **71**, 3.

25 M. J. Frisch, G. W. Trucks, H. B. Schlegel, G. E. Scuseria, M. A. Robb, J. R. Cheeseman, G. Scalmani, V. Barone, B. Mennucci, G. A. Petersson, H. Nakatsuji, M. Caricato, X. Li, H. P. Hratchian, A. F. Izmaylov, J. Bloino, G. Zheng, J. L. Sonnenberg, M. Hada, M. Ehara, K. Toyota, R. Fukuda, J. Hasegawa, M. Ishida, T. Nakajima, Y. Honda, O. Kitao, H. Nakai, T. Vreven, J. A. Montgomery Jr, J. E. Peralta, F. Ogliaro, M. Bearpark, J. J. Heyd, E. Brothers, K. N. Kudin, V. N. Staroverov, R. Kobayashi, J. Normand, K. Raghavachari, A. Rendell, J. C. Burant, S. S. Iyengar, J. Tomasi, M. Cossi, N. Rega, M. Millam, M. Klene, J. E. Knox, J. B. Cross, V. Bakken, C. Adamo, J. Jaramillo, R. Gomperts, R. E. Stratmann, O. Yazyev, A. J. Austin, R. Cammi, C. Pomelli, J. W. Ochterski, R. L. Martin, K. Morokuma, V. G. Zakrewski, G. A. Voth, P. Salvador, J. J. Dannenberg, S. Dapprich, A. D. Daniels, Ö. Farkas,

J. B. Foresman, J. V. Ortiz, J. Cioslowski and D. J. Fox, *Gaussian 09 (Revision B. 01)*, Gaussian, Inc., Wallingford, CT, 2010.

26 (*a*) V. A. Rassolov, M. A. Ratner, J. A. Pople, P. C. Redfern and L. A. Curtiss, *Comput. Chem. J.*, 2001, **22**, 976–984; (*b*) M. M. Francl, W. J. Pietro, J. Hehre, J. S. Binkley, D. J. DeFrees, J. A. Pople and M. S. Gordon, *J. Chem. Phys.*, 1982, **77**, 3654–3665; (*c*) P. C. Hariharan and J. A. Pople, *Theor. Chim. Acta*, 1973, **28**, 213–222; (*d*) W. J. Hehre, R. Ditchfield and J. A. Pople, *J. Chem. Phys.*, 1972, **56**, 2257–2261.

27 (*a*) A. D. Becke, *J. Chem. Phys.*, 1993, **98**, 5648–5652; (*b*) C. Lee, W. Yang and R. G. Parr, *Phys. Rev. B: Condens. Matter Mater. Phys.*, 1988, **37**, 785–789.

28 (*a*) P. J. Hay and W. R. Wadt, *J. Chem. Phys.*, 1985, **82**, 270–283; (*b*) W. R. Wadt and P. J. Hay, *J. Chem. Phys.*, 1985, **82**, 284–298; (*c*) P. J. Hay and W. R. Wadt, *J. Chem. Phys.*, 1985, **82**, 299–310.

29 H. Iguchi, S. Tanaka, Y. Ozawa, T. Kashiwakuma, T. Kimura, T. Hiraga, H. Ozawa and A. Kono, *Cancer Res.*, 1996, **56**, 4040–4043.

30 J. A. Barltrop, T. C. Owen, A. H. Cory and J. G. Cory, *Bioorg. Med. Chem. Lett.*, 1991, **1**, 611–614.

31 M. V. Berridge and A. S. Tan, *Arch. Biochem. Biophys.*, 1993, **302**, 474–482.

32 S. P. Dash, S. Pasayat, S. Bhakat, S. Roy, R. Dinda, E. R. T. Tiekink, S. Mukhopadhyay, S. K. Bhutia, M. R. Harrdikar, B. N. Joshi, Y. P. Patil and M. Nethaji, *Inorg. Chem.*, 2013, **52**, 14096–14107.

33 G. M. Morris, R. Huey, W. Lindstrom, M. F. Sanner, R. K. Below, D. S. Goodsell and A. J. Olson, *J. Comput. Chem.*, 2009, **30**, 2785–2791.

34 W. L. DeLano, *The PyMOL molecular graphics system*, DeLano Scientific, San Carlos, CA, USA, 2002.

35 S. Khatua, A. K. Dutta, S. Chandra, S. Paloi, K. Das and K. Acharya, *PLoS One*, 2017, **12**(5), e0178050.

36 C. Yuan, L. Lu, X. Gao, Y. Wu, M. Guo, Y. Li, X. Fu and M. Zhu, *J. Biol. Inorg. Chem.*, 2009, **14**, 841–851.

37 G. R. Hausen, T. A. Kabanos, A. D. Keramidas, D. Mentzafos and A. Terzis, *Inorg. Chem.*, 1992, **31**, 2587–2594.

38 G. Chen, D. Zhou, X.-Z. Li, Z. Jiang, C. Tan, X.-Y. Wei, J. Ling, J. Jing, F. Liu and N. Li, *Sci. Rep.*, 2017, **7**, 10729, DOI: 10.1038/s41598-017-11369.

39 (*a*) N. Sepay, S. Mallik, C. Guha and A. K. Mallik, *RSC Adv.*, 2016, **6**, 96016–96024; (*b*) N. Sepay, C. Guha, S. Maity and A. K. Mallik, *Eur. J. Org. Chem.*, 2017, 6013–6022.

40 M. Inoue, K. Segawa, S. Matsunaga, N. Matsumoto, M. Oda and T. Yamase, *J. Inorg. Biochem.*, 2005, **99**, 1023–1031.

41 M. N. Patel, S. H. Patel, M. R. Chhasatia and P. A. Parmar, *Bioorg. Med. Chem. Lett.*, 2008, **18**, 6494–6500.

42 M. K. Sahini, U. Yadava, O. P. Pandey and S. K. Sengupta, *Spectrochim. Acta, Part A*, 2014, **125**, 189–194.

43 M. R. Maurya, A. Kumar, A. R. Bhat, A. Azam, C. Bader and D. Rehder, *Inorg. Chem.*, 2006, **45**, 1260–1269.